

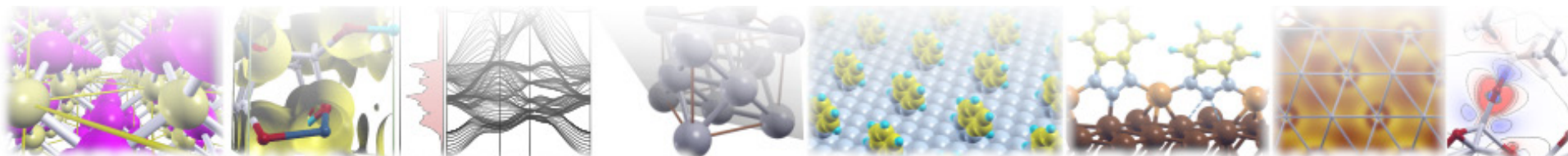


QUANTUM ESPRESSO

September 15–20, 2019

Ljubljana, Slovenia

Summer School on Advanced Materials and Molecular Modelling



Elevator pitches (part I)



DFT calculation of dielectric properties for alloys

Matej Bubaš

Dr. sc. Jordi Sancho Parramon

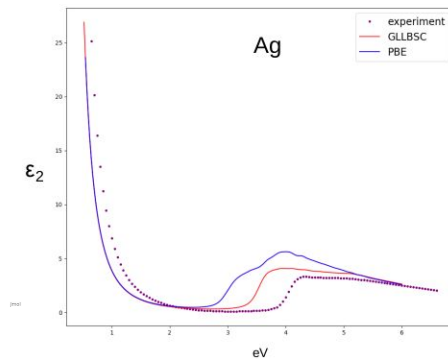
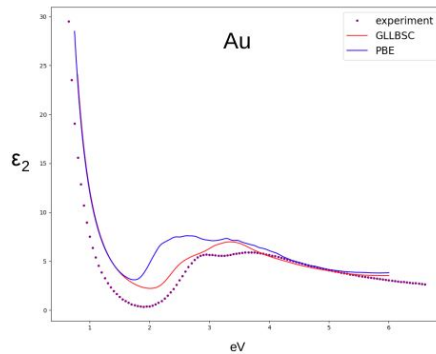
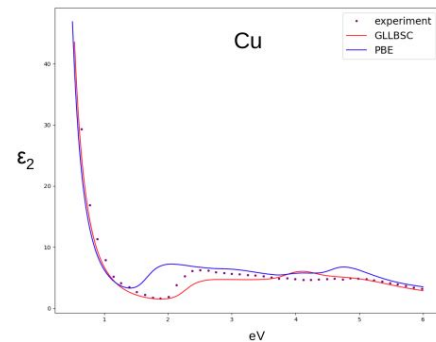
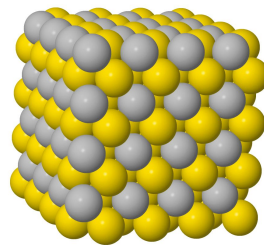
Ruđer Bošković Institute, Zagreb, Croatia

Overview

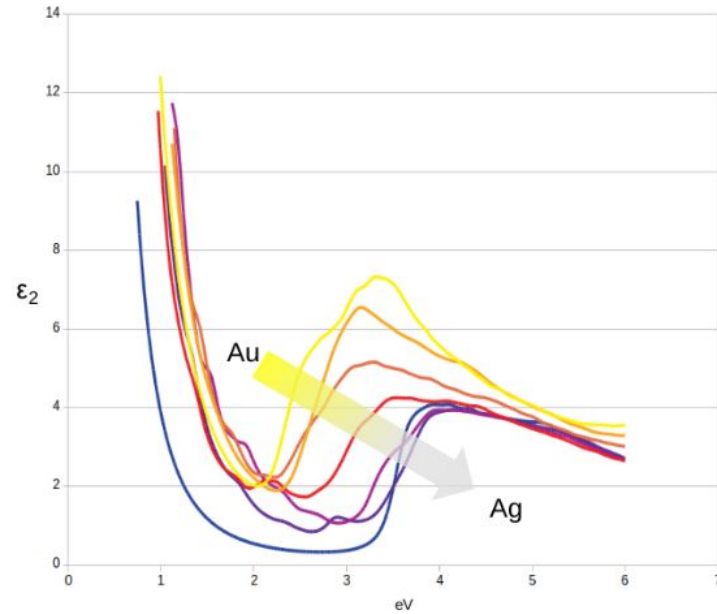
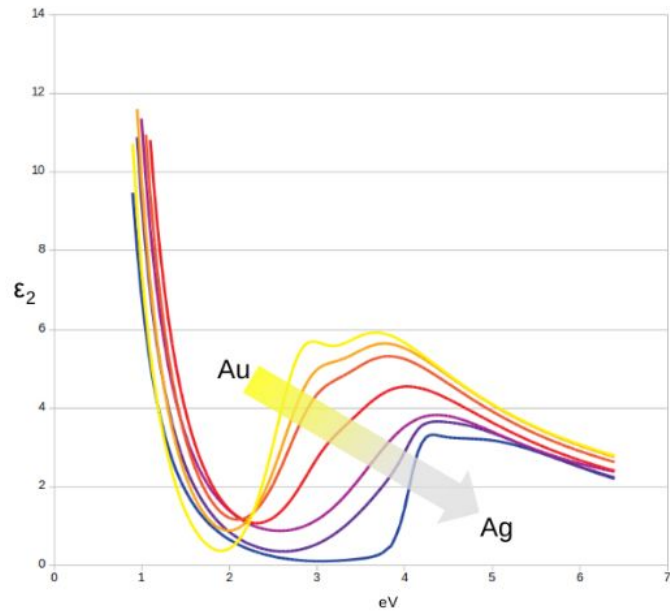
Goal: To find a computationally inexpensive way of predicting how dielectric function changes with alloy composition.

Why: Avoiding a lot of cumbersome experiments. Results are especially useful in the field of plasmonics.

How: Using supercells with atomic ratio that corresponds to desired alloy composition and finding the best parameters for inexpensive calculations so avoiding expensive corrections can be tolerable.



Results



Shall I compare thee to a summer's day...

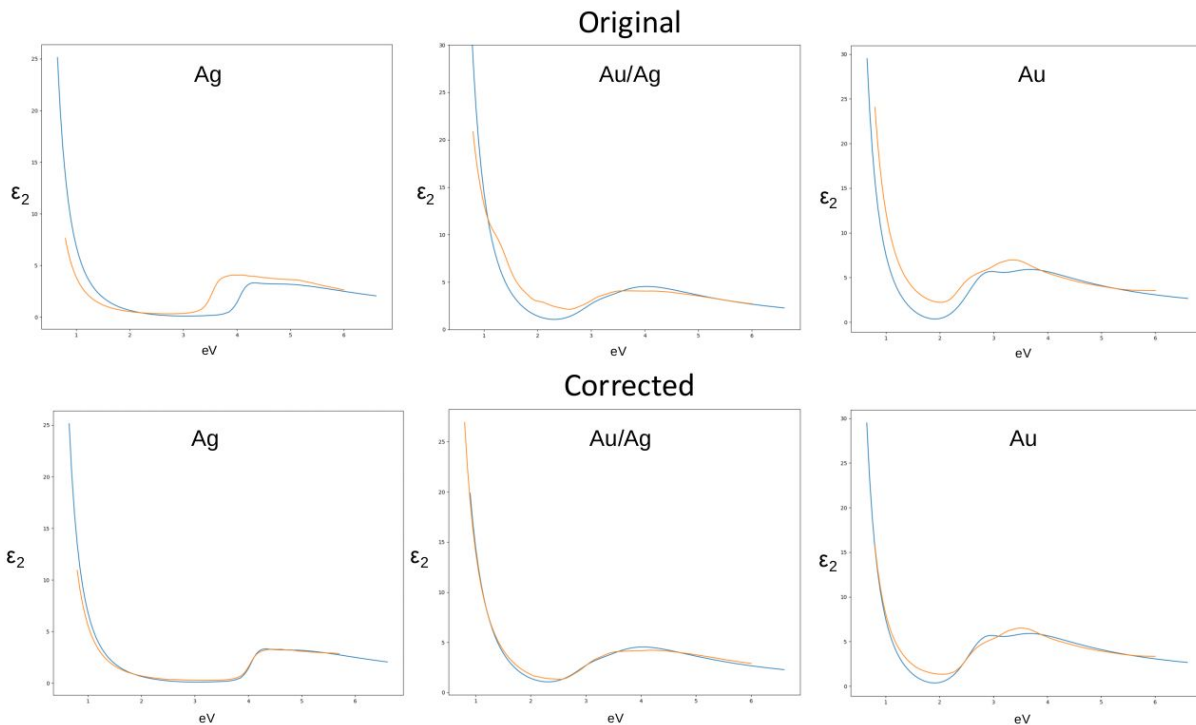


What's next

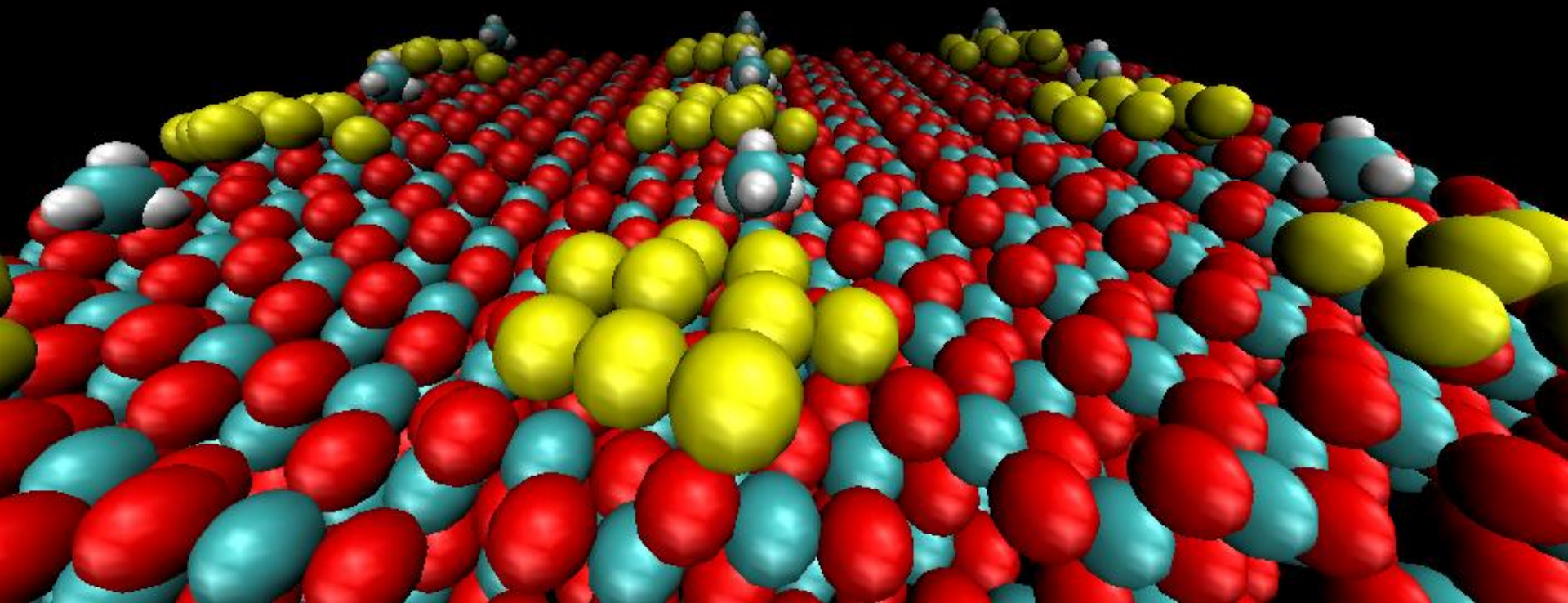
Using a fitting algorithm that corrects the DFT dielectric function using minimal empirical data. Tracking how parameters change and inferring why.

Calculating corresponding dielectric functions for spherical nanoparticles using Mie theory and comparing to literature data.

More alloys.



Thank you for your attention!



THE UNIVERSITY
of ADELAIDE

adelaide.edu.au

Co-transformation of methane and water using atomically precise gold clusters on titania

Jenica Marie L. Madrideojos
jenicamarie.madrideojos@adelaide.edu.au

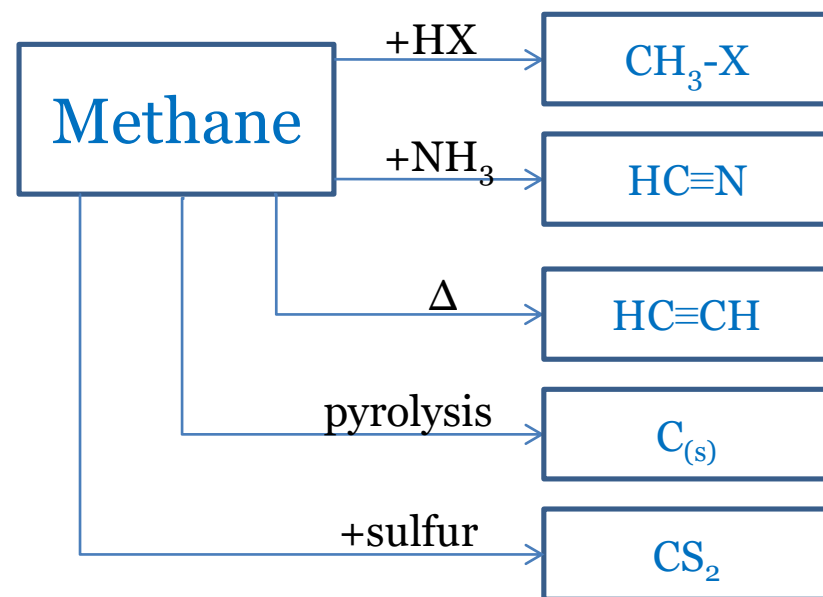
seek LIGHT

Methane

- Major component of natural gas
- Behaves like molecular H₂:
C-H bond breaking = **430 kJ/mol**
- Very low chemical reactivity, 12.6 eV to ionize
- Higher global warming potential (GWP) than CO₂ (**25 x worse**)
- A good source of H₂ gas, a cleaner fuel than gasoline, easily transported

Methane

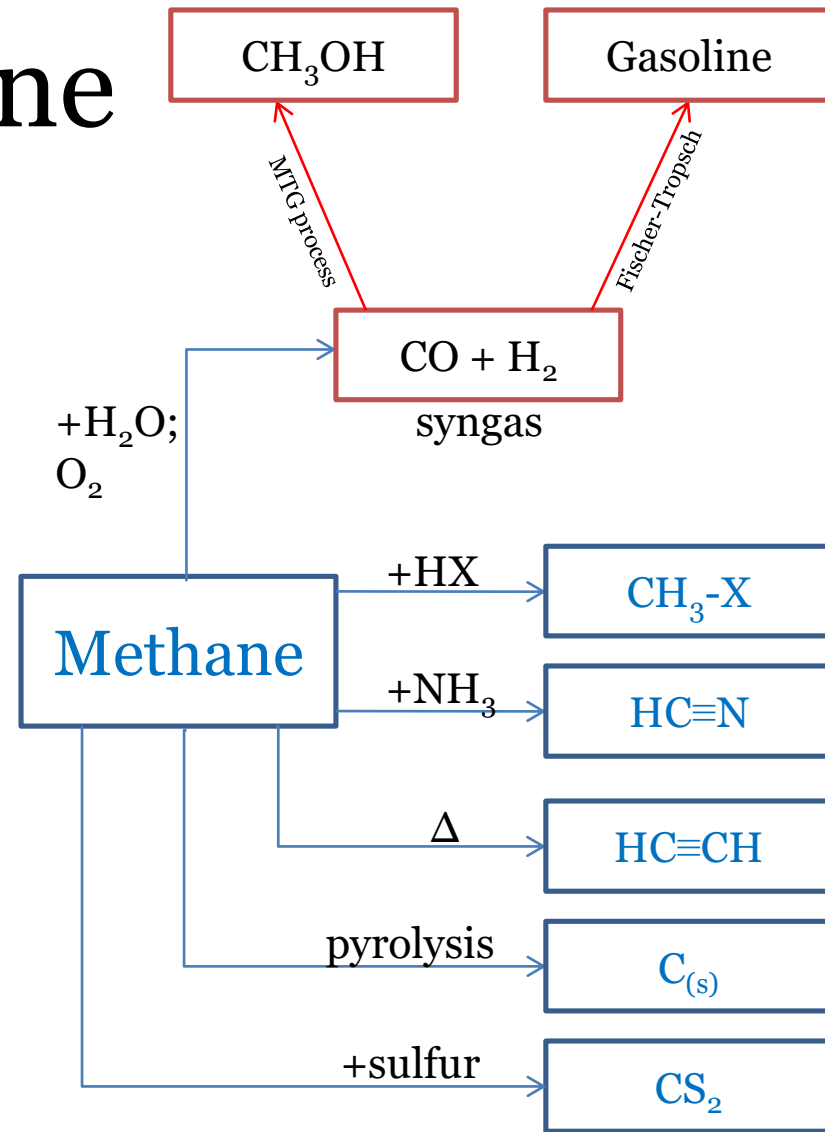
- Major component of natural gas
- Behaves like molecular H_2 :
C-H bond breaking = **430 kJ/mol**
- Very low chemical reactivity, 12.6 eV to ionize
- Higher global warming potential (GWP) than CO_2 (**25 x worse**)
- A good source of H_2 gas, a cleaner fuel than gasoline, easily transported



Scheme 1. Uses of natural gas in industrial processes.

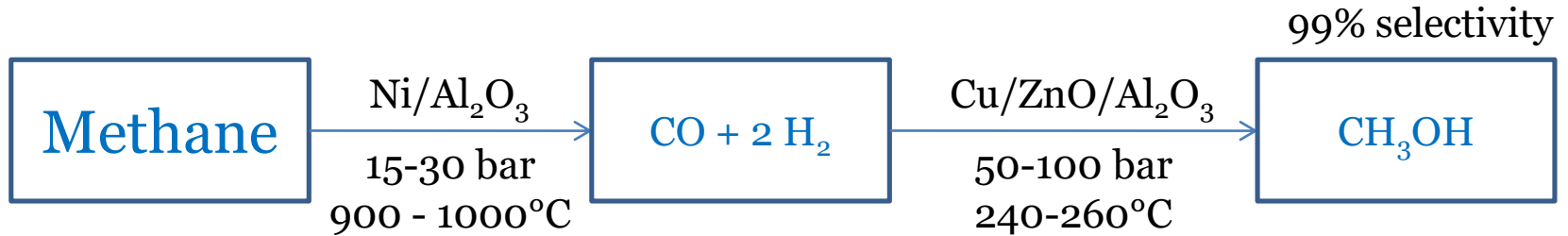
Methane

- Major component of natural gas
- Behaves like molecular H_2 :
C-H bond breaking = **430 kJ/mol**
- Very low chemical reactivity, 12.6 eV to ionize
- Higher global warming potential (GWP) than CO_2 (**25 x worse**)
- A good source of H_2 gas, a cleaner fuel than gasoline, easily transported

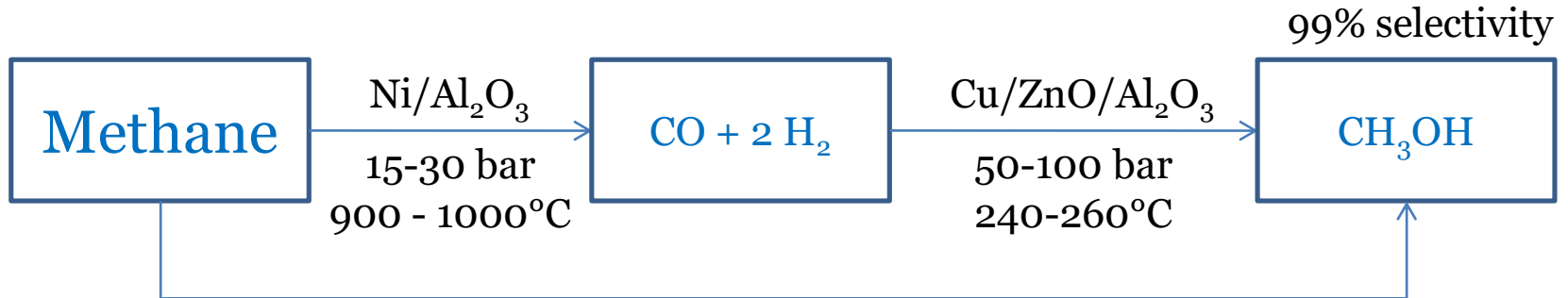


Scheme 1. Uses of natural gas in industrial processes.

Methane conversion

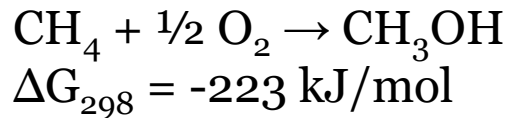
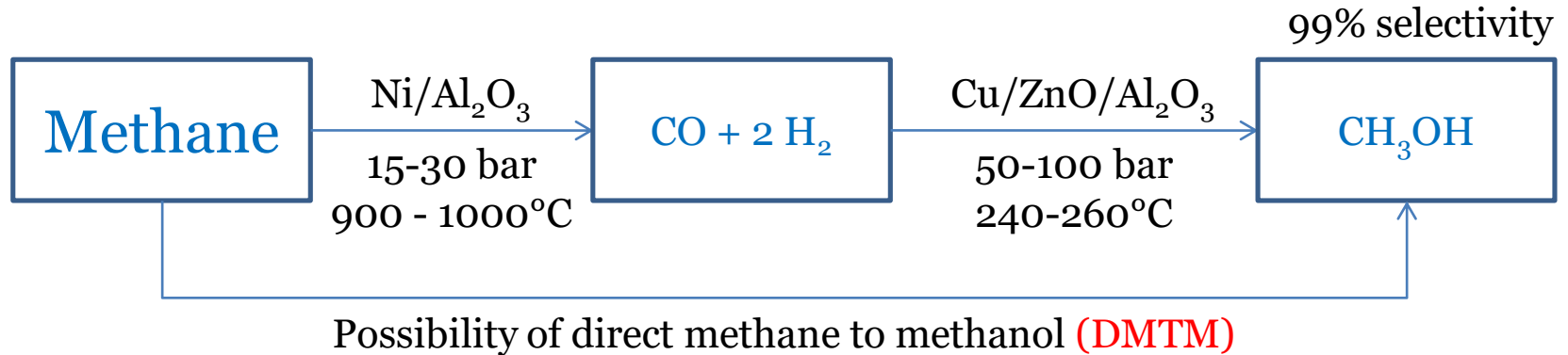


Methane conversion



Possibility of direct methane to methanol (DMTM)

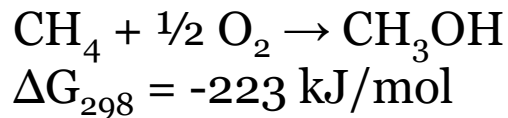
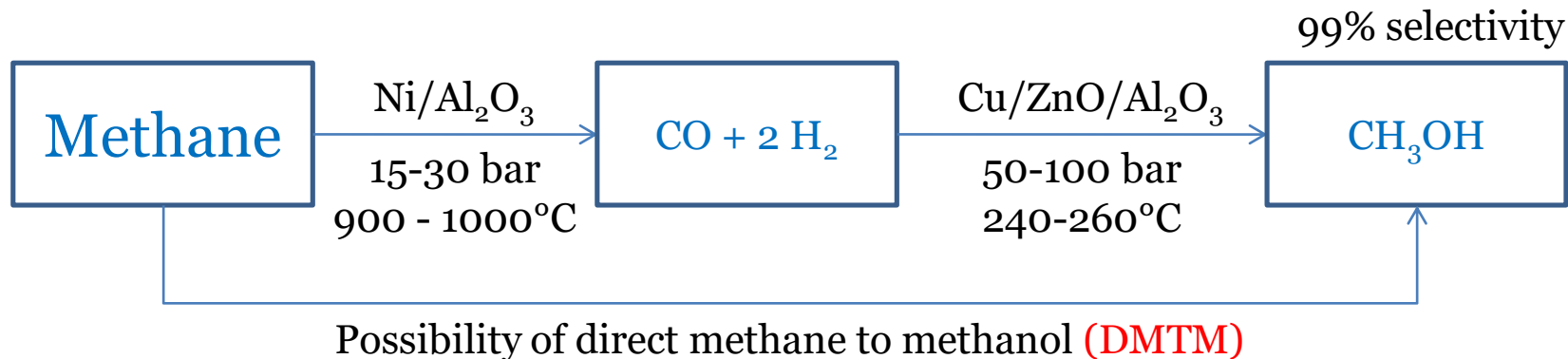
Methane conversion



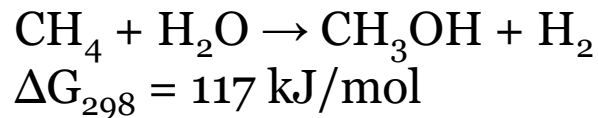
Con:

MeOH produced oxidized easily
to CO₂ when excess O₂ is present

Methane conversion



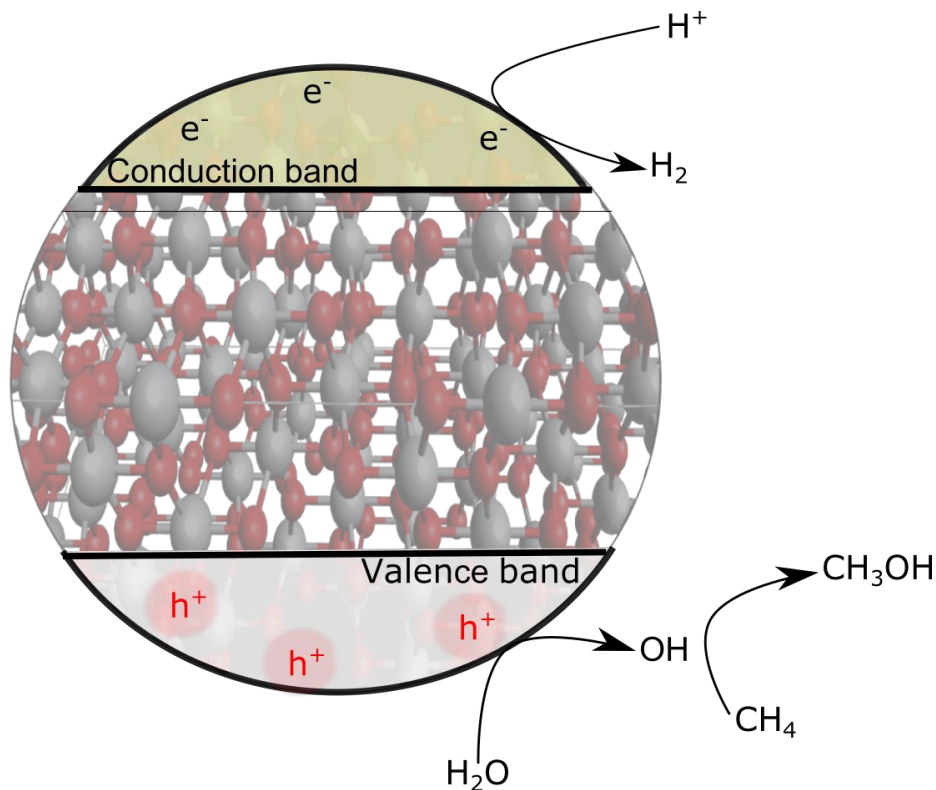
Con:
MeOH produced oxidized easily
to CO₂ when excess O₂ is present



Con:
Needs higher amount of energy
for reaction to proceed.
 $\Delta H = 124 \text{ kJ/mol}$

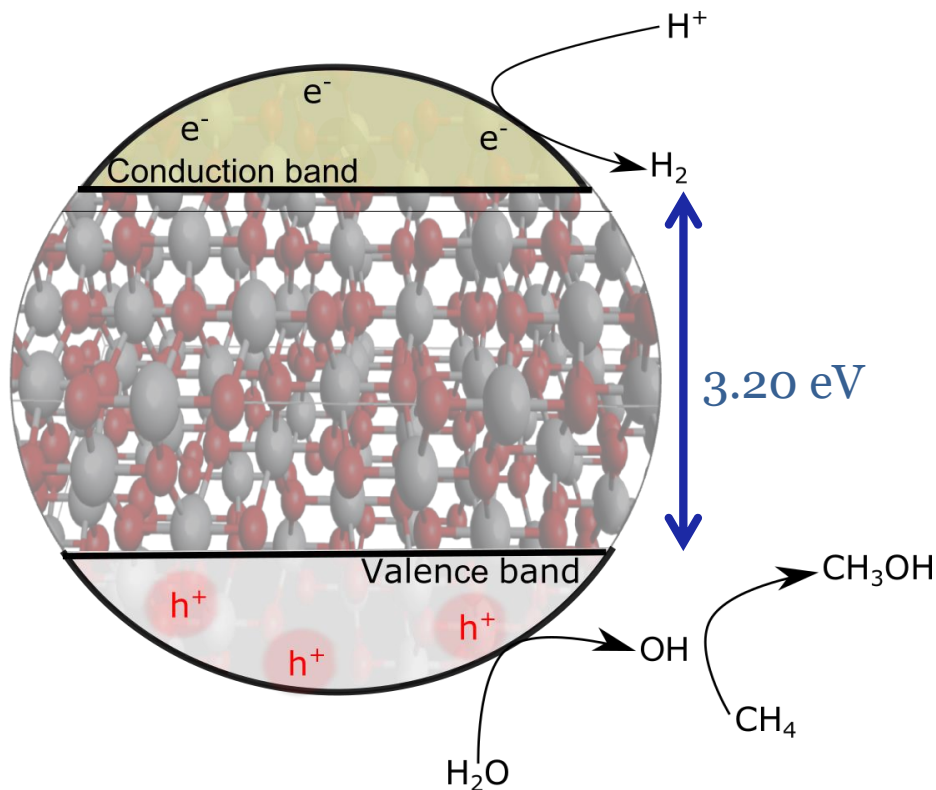
Photocatalysis

- photocatalysts are semiconductors, from micron-sized powders to nanoparticles, that involve electron transfer from their valence band to conduction band.



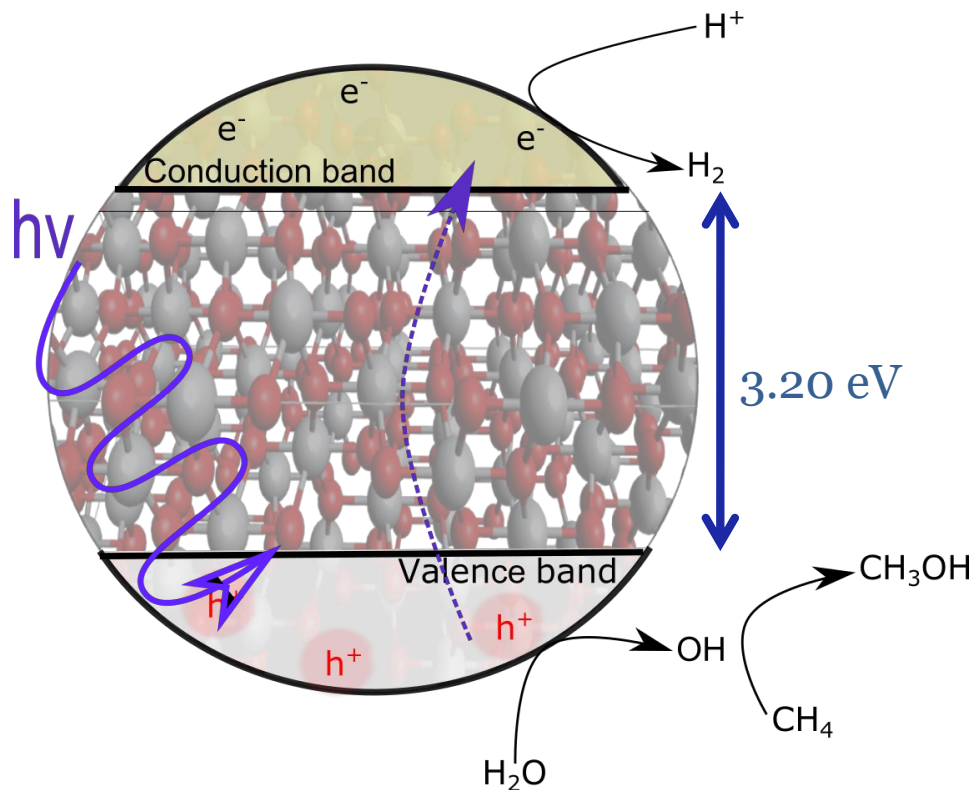
Photocatalysis

- photocatalysts are semiconductors, from micron-sized powders to nanoparticles, that involve electron transfer from their valence band to conduction band.



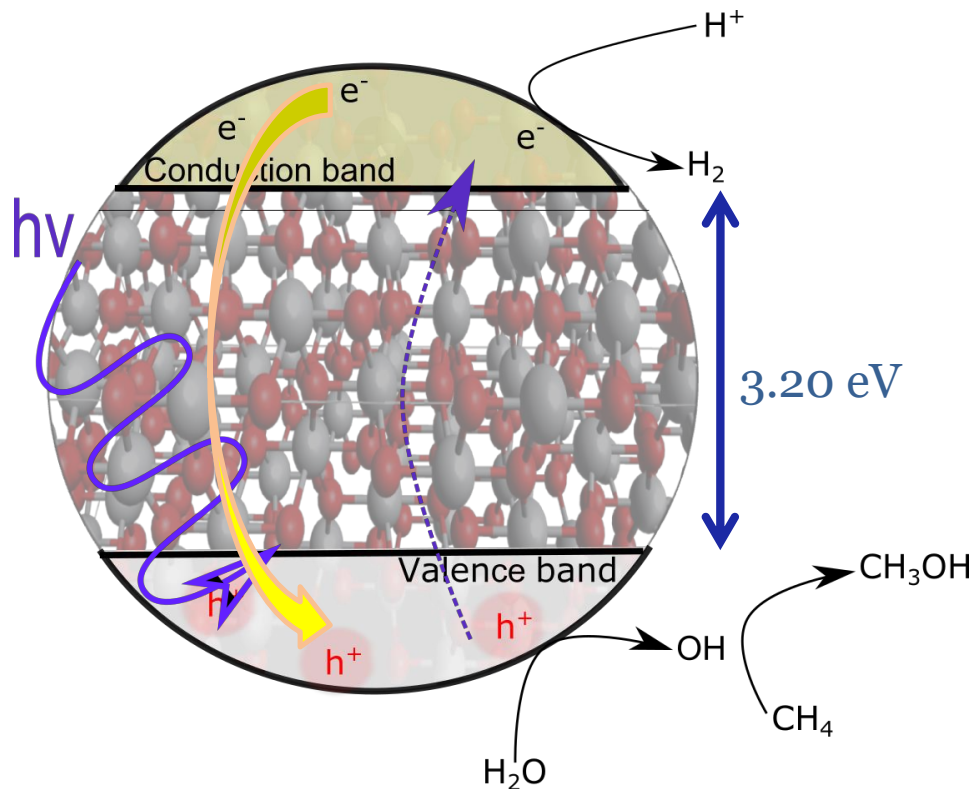
Photocatalysis

- photocatalysts are semiconductors, from micron-sized powders to nanoparticles, that involve electron transfer from their valence band to conduction band.



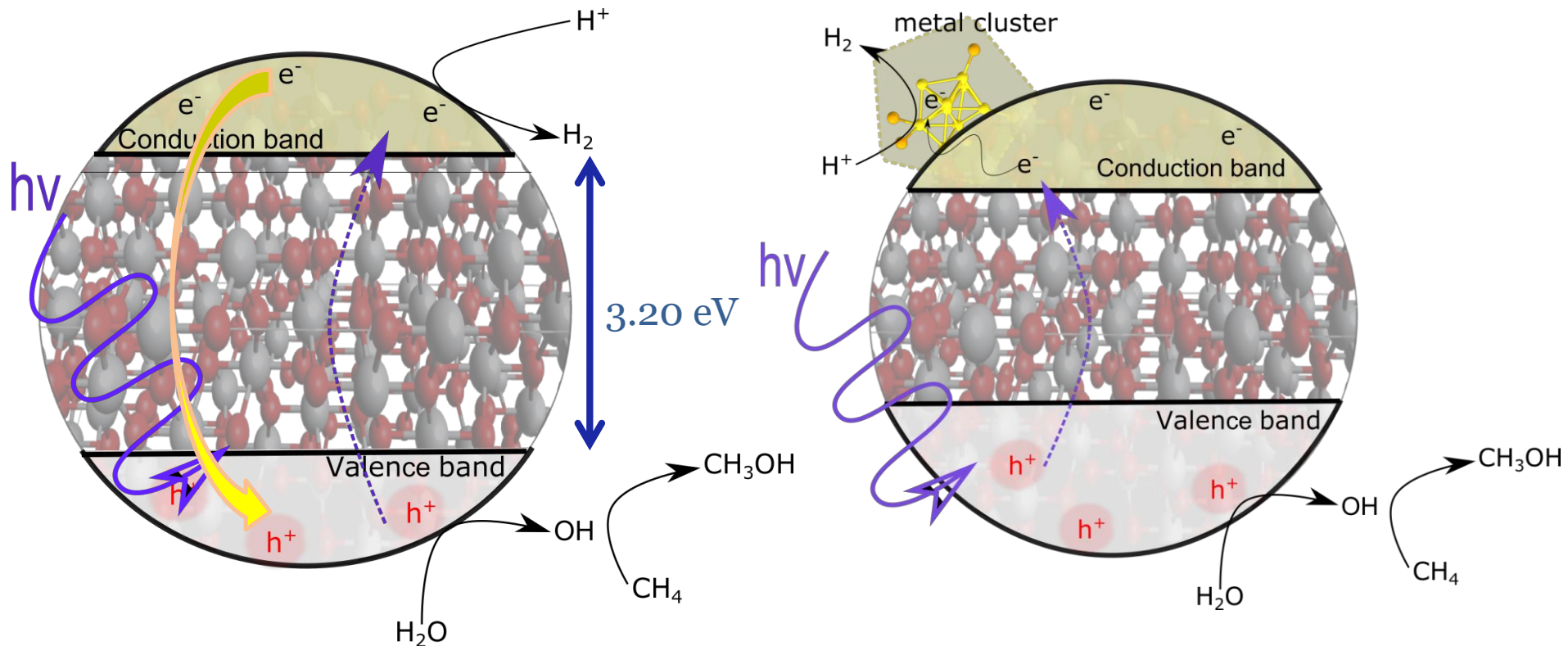
Photocatalysis

- photocatalysts are semiconductors, from micron-sized powders to nanoparticles, that involve electron transfer from their valence band to conduction band.



Photocatalysis

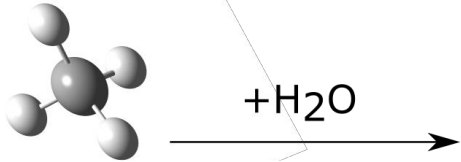
- photocatalysts are semiconductors, from micron-sized powders to nanoparticles, that involve electron transfer from their valence band to conduction band.



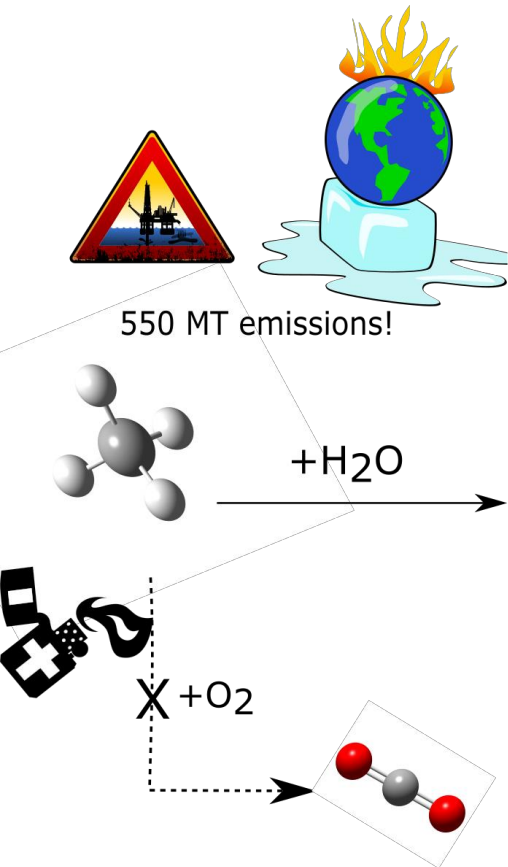
Summary of this research project



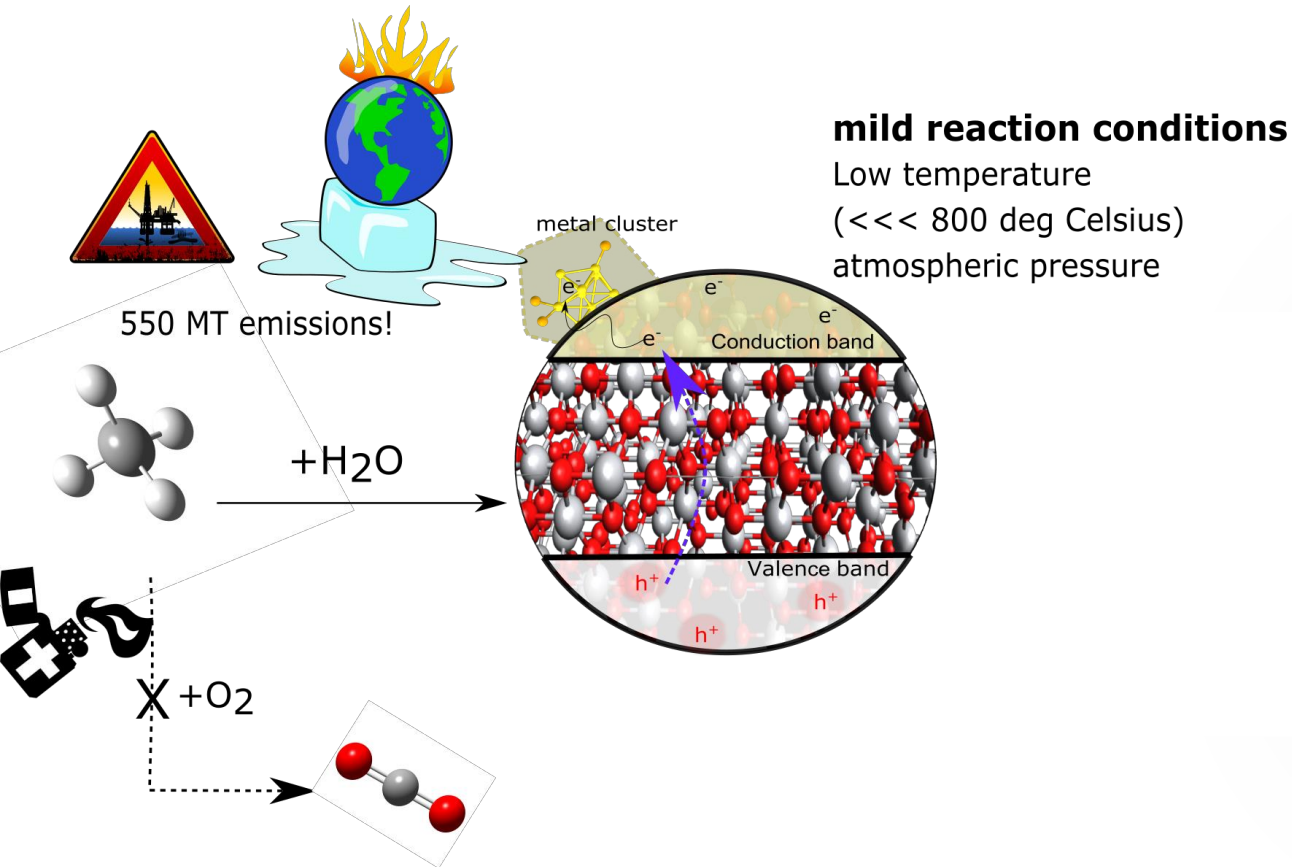
550 MT emissions!



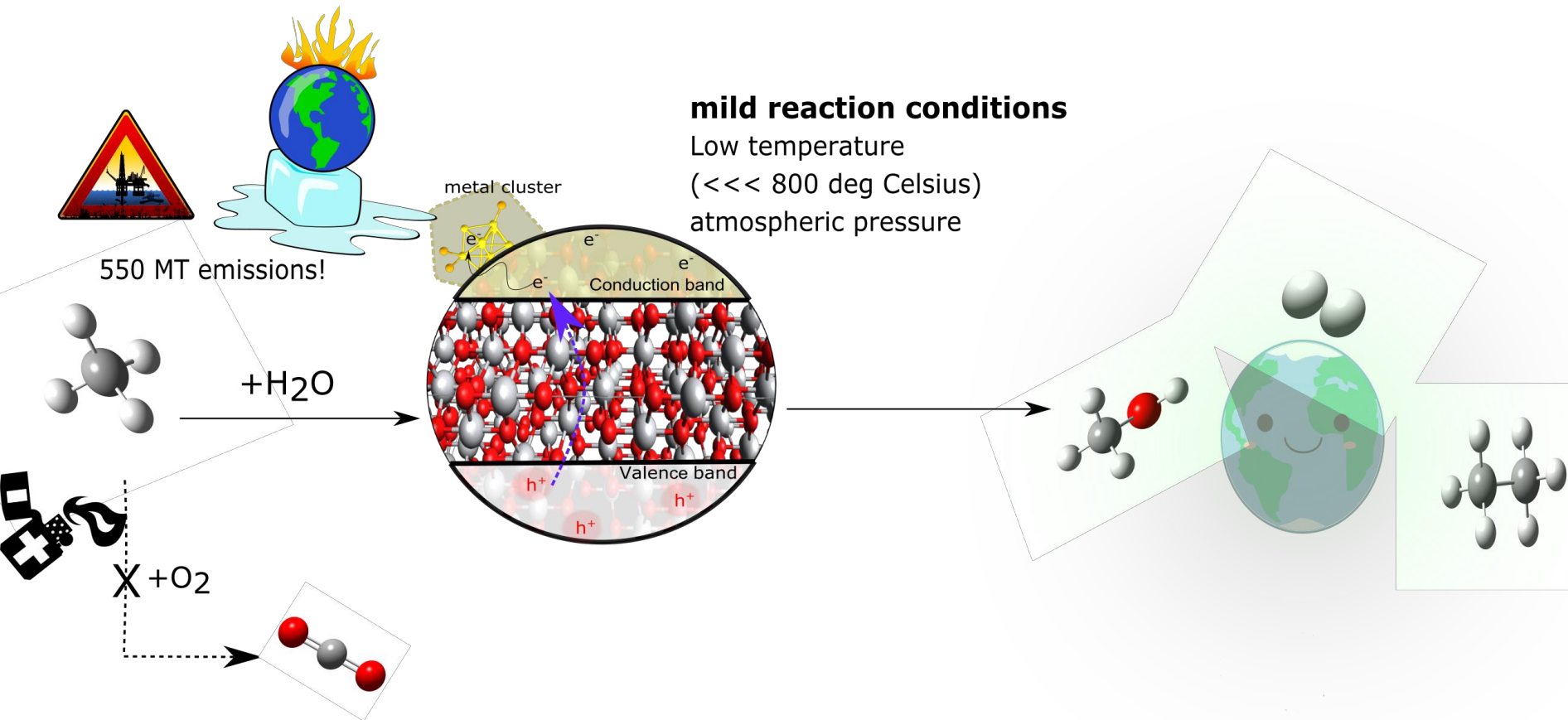
Summary of this research project



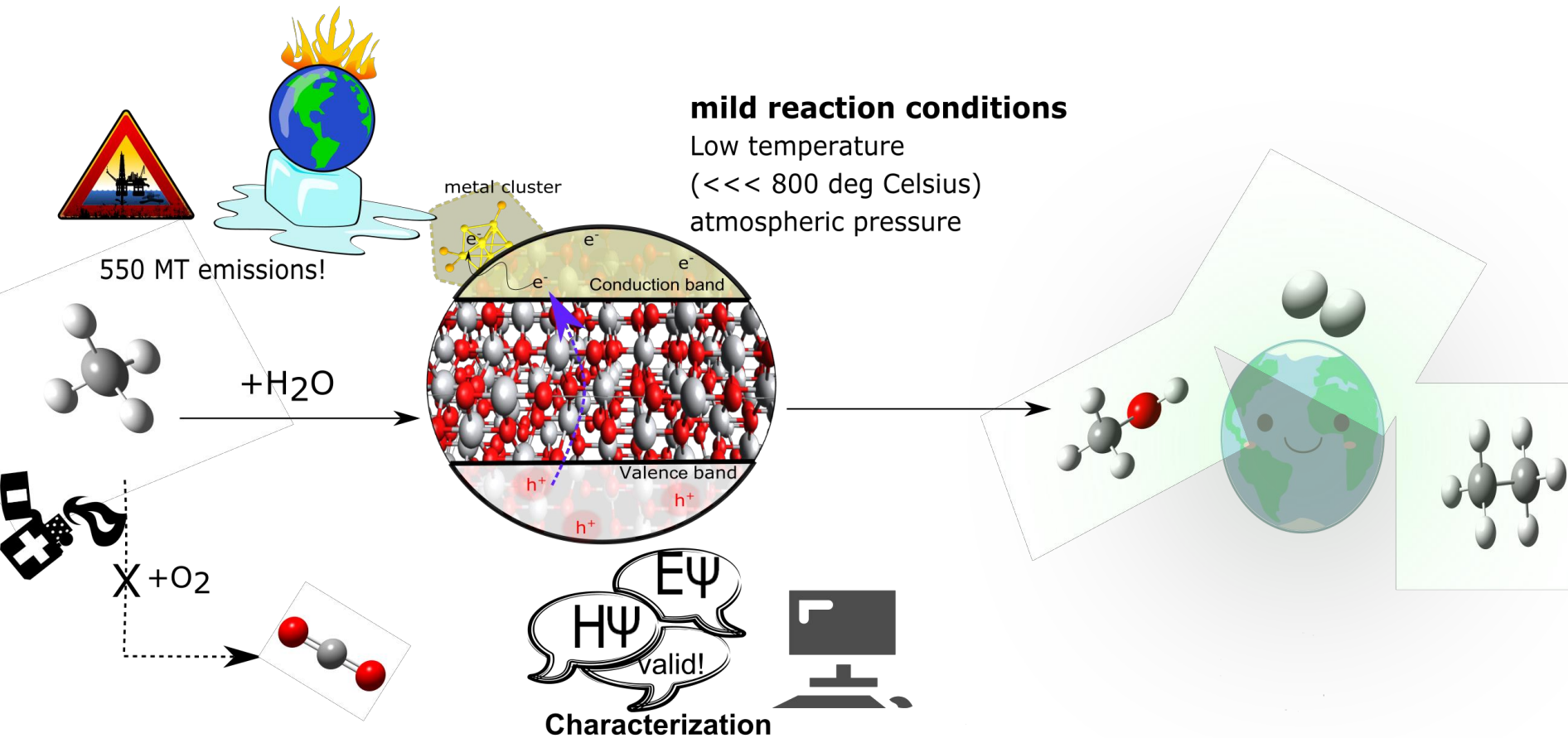
Summary of this research project



Summary of this research project



Summary of this research project

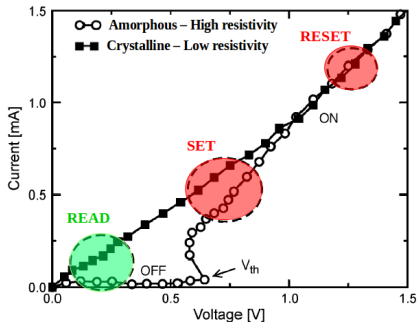


A first principles study of the switching mechanism in InSbTe-GeTe superlattices

Chiara Ribaldone, Daniele Dragoni, Marco Bernasconi

Phase Change Memories (PCMs)

- Fast (50 - 100 ns) and reversible transition between the amorphous and the crystalline states (Joule heating)
- Difference of resistivity between amorphous - crystalline states $\sim 10^3$
- Chalcogen alloys: GeTe, $\text{Ge}_2\text{Sb}_2\text{Te}_5$ (GST), In_3SbTe_2



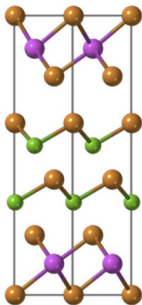
RESET:
crystal \rightarrow liquid \rightarrow amorphous
high currents, short pulses

SET:
amorphous \rightarrow crystal
low currents, long pulses

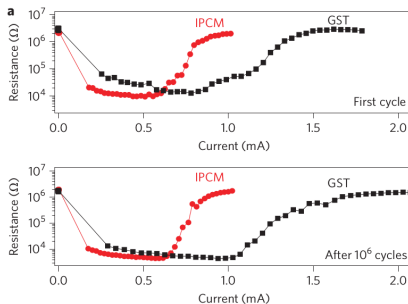
Read out is performed at low bias

Interfacial Phase Change Memories (IPCMs)

- IPCMs are based on $\text{Sb}_2\text{Te}_3(\text{GeTe})_2$ superlattices with blocks of Sb_2Te_3 alternated to GeTe blocks
- Low programming current with respect to GST-based PCMs \rightarrow higher efficiency



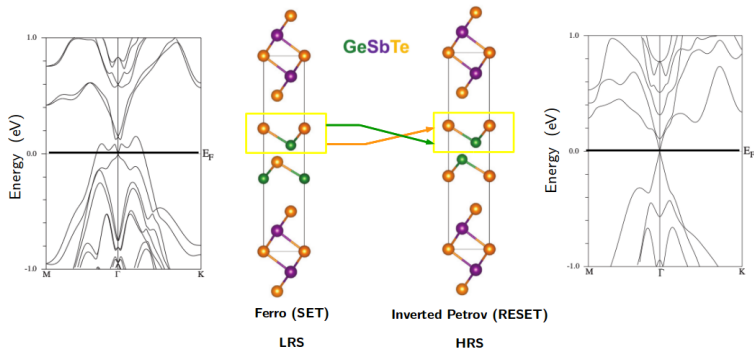
● Ge ● Sb ● Te



R. E. Simpson et al., Nat. Nanotechnol. 6, 501, (2011)

Hypothesis for the transition mechanism in IPCMs

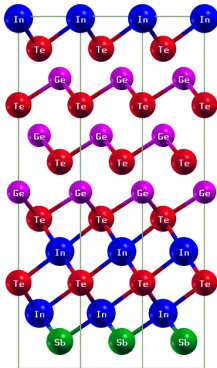
- *Ab-initio* calculations on $\text{Sb}_2\text{Te}_3(\text{GeTe})_2$ identify the low resistance state (LRS) as the Ferro configuration and the high resistance state (HRS) as the Inverted Petrov configuration
→ both the LRS and the HRS are crystalline states
- The HRS and LRS configurations differ by the inversion of the Ge and Te layers in the GeTe block



J. Tominaga et al., Adv. Mater. Interfaces 1, 1300027, (2014)

New IPCM superlattices InSbTe-GeTe

- DFT simulations
- $\text{In}_3\text{SbTe}_2(\text{GeTe})_3$ superlattice shows promising features for application in IPCMs:



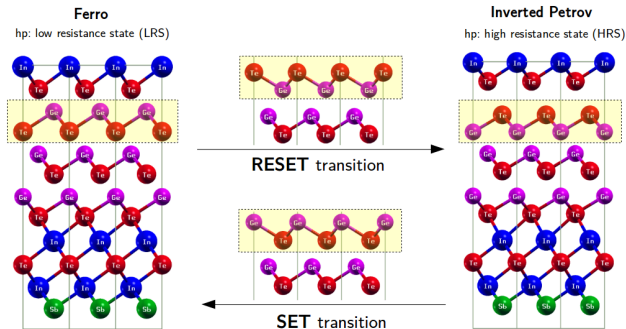
- 1 low formation energy: 19.51 meV/atom
- 2 the structure is locally stable up to 950 K
- 3 in-plane biaxial strain on GeTe: **1.9%**
(0.5% in $\text{Sb}_2\text{Te}_3(\text{GeTe})_2$ ^{[1],[2]}) →

→ **reduction of the energy barrier for the RESET-SET transformations** with respect to $\text{Sb}_2\text{Te}_3(\text{GeTe})_2$ superlattices?

[1] X. Yu et al., *Sci. Rep.* 5, 12612 (2015)

[2] D. Campi et al., *Phys. Rev. B* 95, 024311 (2017)

RESET and SET transitions in $\text{In}_3\text{SbTe}_2(\text{GeTe})_3$ superlattice



■ Nudged Elastic Band (NEB) calculations:

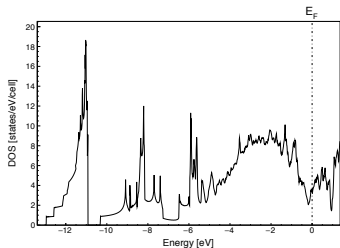
		$\text{Sb}_2\text{Te}_3(\text{GeTe})_2$	$\text{In}_3\text{SbTe}_2(\text{GeTe})_3$	Energy gain [eV]
Activation energy [eV]	RESET	2.56 ^[1]	2.41	0.15
	SET	2.84 ^[1]	1.93	0.91

[1] X. Yu et al., *Sci. Rep.* 5, 12612 (2015)

Conductivity of the Ferro and Inverted Petrov phases - $\text{In}_3\text{SbTe}_2(\text{GeTe})_3$

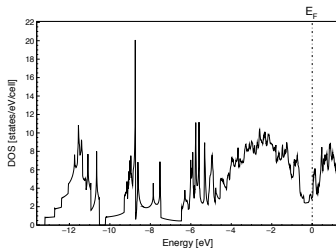
Ferro

$\text{DOS}(E_F) = 3.62 \text{ states/eV/cell}$



Inverted Petrov

$\text{DOS}(E_F) = 2.98 \text{ states/eV/cell}$



- Boltzmann equation of transport, constant relaxation time approximation:

$$\sigma_{\mu\nu} \propto \sum_{\alpha, \mathbf{k}} \mathbf{v}_{\mu}(\alpha, \mathbf{k}) \mathbf{v}_{\nu}(\alpha, \mathbf{k}) \delta(\varepsilon_F - \varepsilon_{\alpha}(\mathbf{k}))$$

- Ratio between the conductivity of the Ferro and the Inverted Petrov configurations:

$$\sigma_{zz}^{\text{Ferro}} / \sigma_{zz}^{\text{Inverted Petrov}} = 2.5 \quad \text{along the direction of superlattice growth}$$

DFT calculations:

- a **strain** of 1.9% in the GeTe block of $\text{In}_3\text{SbTe}_2(\text{GeTe})_3$ superlattice **reduces the energy barrier for the RESET-SET transitions** with respect to $\text{Sb}_2\text{Te}_3(\text{GeTe})_2$ superlattices by 0.15 eV and by 0.91 eV for the RESET and the SET transitions, respectively
- in $\text{In}_3\text{SbTe}_2(\text{GeTe})_3$ superlattice the **Ferro configuration** has **higher conductivity than the Inverted Petrov phase**
- the **contrast in conductivity** between the Ferro and Inverted Petrov phases seems to be **too low** to distinguish between two states of memory 1/0, but **further calculations with spin-orbit coupling are needed** to better assess the values of the conductivity of the two configurations

Thank you for your attention!

SCRUTINIZING THE BONDING OF 2-MERCAPTOBENZIMIDAZOLE ON Cu(111) BY STM AND DFT



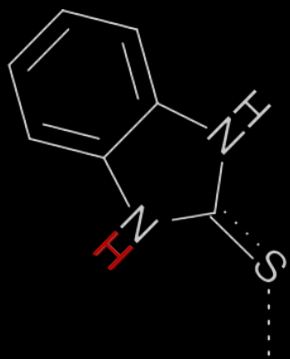
Marion A. van Midden, Matic Lozinšek, Erik Zupanič, Anton Kokalj

WHY?

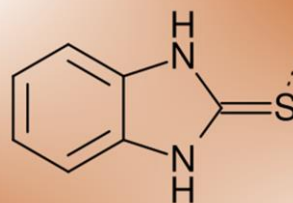
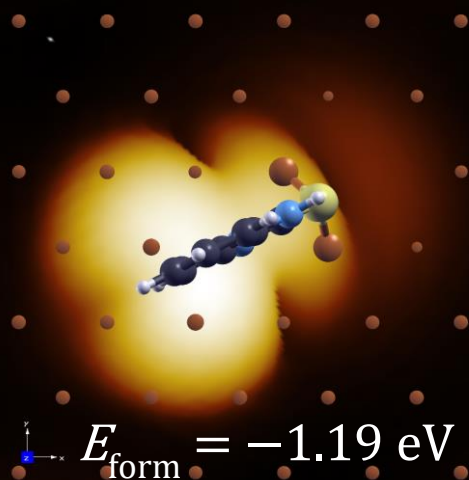
- Understanding corrosion inhibition.
- How do they bind to the surface?
- Which interactions are important?

HOW?

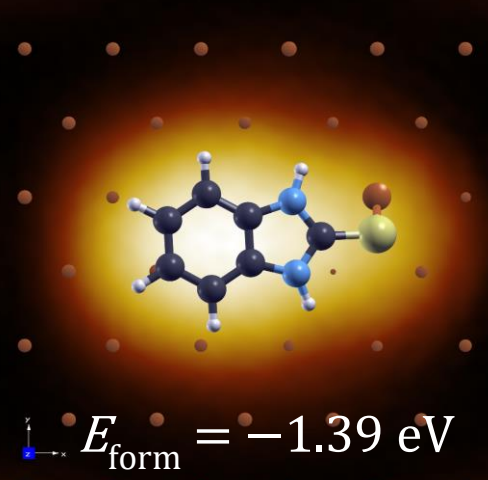
Density Functional Theory



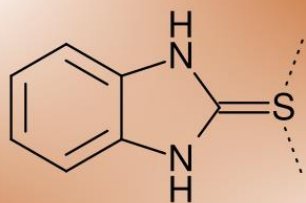
Cu(111)



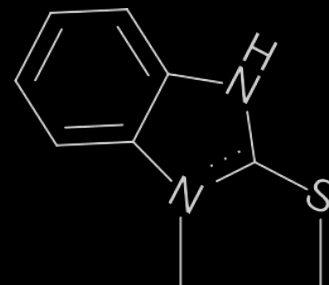
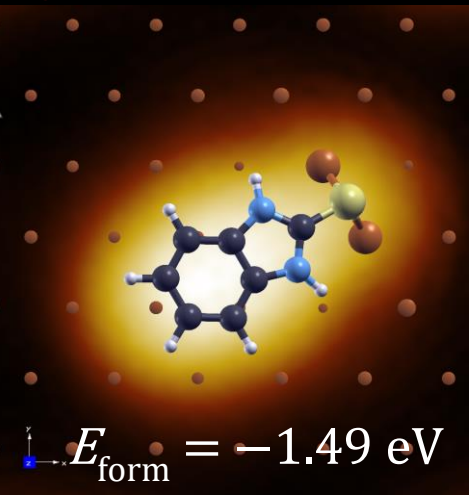
Cu(111)



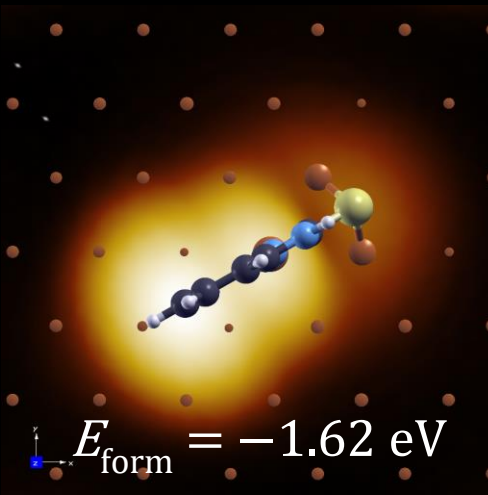
Similar binding energies!



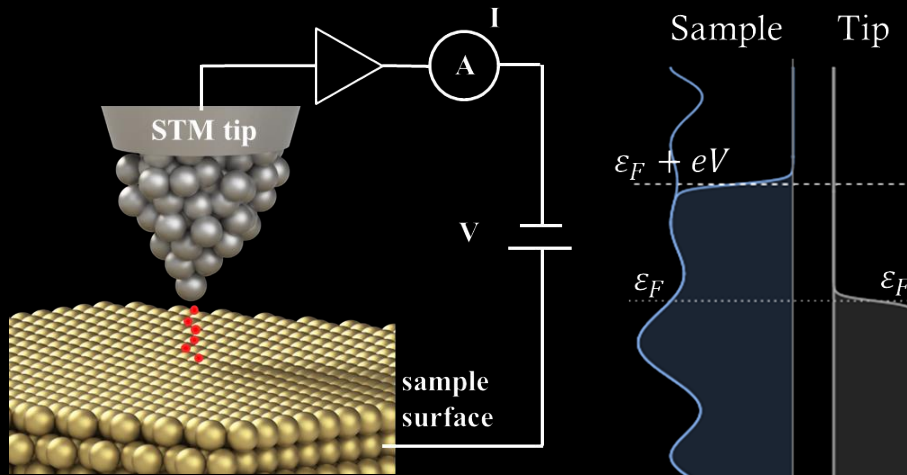
Cu(111)



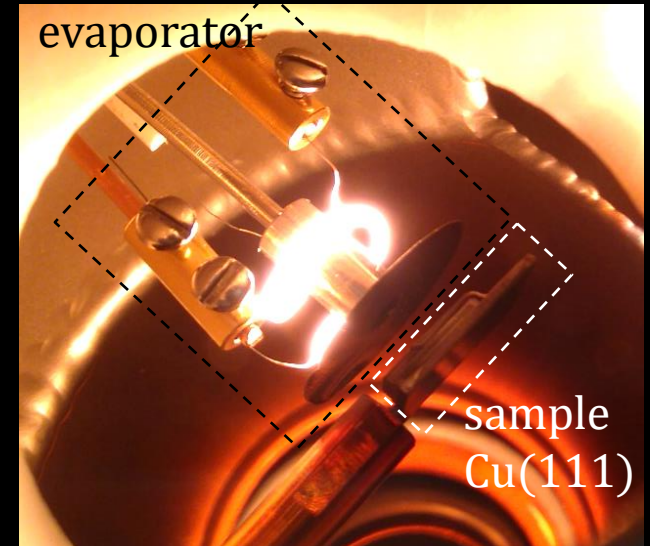
Cu(111)



Scanning Tunneling Microscopy



$$I \propto e^{-\kappa z} \rho_T(0) \int_0^{eV} \rho_S(\varepsilon) d\varepsilon$$



- Ultra high vacuum
- Low temperatures (4.2 K or 1.2 K)



- Anticorrosives in UHV?

SCRUTINIZING THE BONDING OF 2-MERCAPTOBENZIMIDAZOLE ON Cu(111) BY STM AND DFT



Marion A. van Midden, Matic Lozinšek, Erik Zupanič, Anton Kokalj

WHY?

- Understanding corrosion inhibition.
- How do they bind to the surface?
- Which interactions are important?

HOW?

- Combining STM and DFT

RESULTS?

SCRUTINIZING THE BONDING OF 2-MERCAPTOBENZIMIDAZOLE ON Cu(111) BY STM AND DFT

Marion A. van Midden, Matic Lozinšek, Erik Zupanič, Anton Kokalj

Condensed Matter Physics Department F3 & Physical and Organic Chemistry Department F3
Jozef Stefan Institute, Jamova 39, 1000 Ljubljana, Slovenia

WHY?

- Understanding corrosion inhibition.
- How they bind to the surface?
- Which interactions are important?

Interaction	Energy	Range (Å)
Van der Waals	-0.1 eV	> 3.0
Hydrogen bonds	0.1-0.5 eV	1.5-2.0
Hydrogen bonds	0.1-0.7 eV	0.15-0.35
Hydrophobic	0.1-0.2 eV	0.3-0.5
Electrostatic	0.1-0.2 eV	0.1-0.5
Substrate adsorption	> 0.1 eV	0.1 to 0.2 nm

HOW?

Density Functional Theory

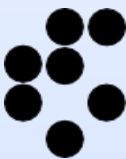
- Different evaporation conditions, respectively, result in many different structures.
- High mobility on the surface even at low temperatures.

Scanning Tunneling Microscopy

$$I = \int_{-\infty}^{\infty} e^{-\kappa|z|} \rho_s(z) dz$$

- Competing interactions have similar energies.
- Selective binding to specific sites is not observed.
- Multiple adsorption on the surface is important.
- Not only attractive, also repulsive interactions need to be considered.

SAMPLE PREPARATION



Superhydrophobic surface on aluminium based on alkyl and perfluoroalkyl



Dr. Peter Rodič, prof. dr. Ingrid Milošev



Motivation

MOTIVATION

THEORY

Superhydrophobic surface has attracted much attention because its special functions:

- water-repellency,
- anti-corrosion
- and anti-icing properties.

PREPARATION

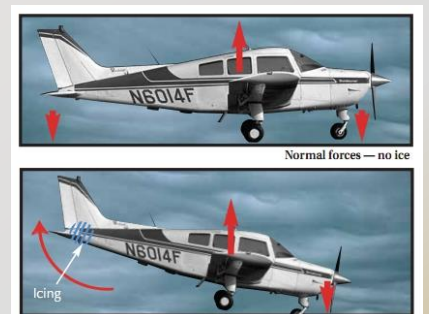
Smart coatings are special films with predefined properties that make them sense and respond to environmental and other external stimuli.

RESULTS

- Corrosion protection
- Self-cleaning coating
- Anti-icing coating

Typical smart coatings are:

- Self-assembling
- Self-healing
- Self-cleaning



CONCLUSIONS



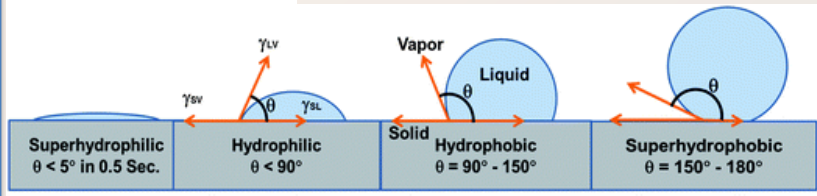
Hydrophobicity

MOTIVATION

Hydrophobicity is usually characterized by water contact angle (WCA) and sliding angle (SA).

THEORY

Contact angle



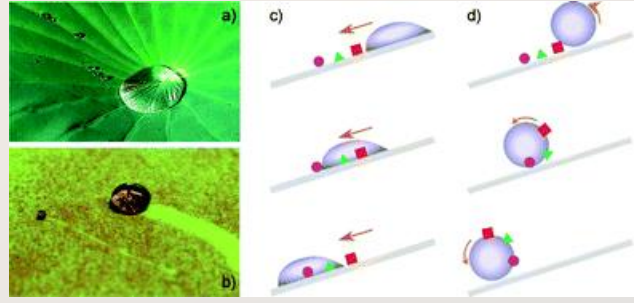
PREPARATION

RESULTS

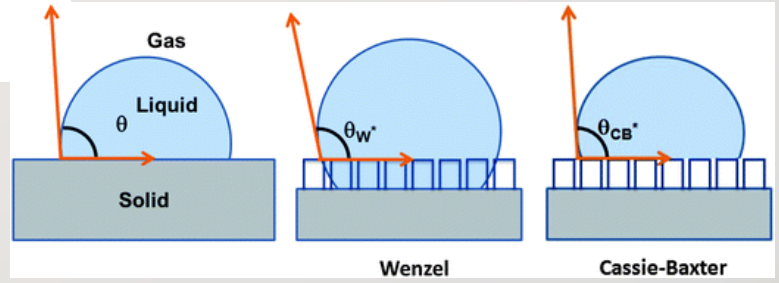
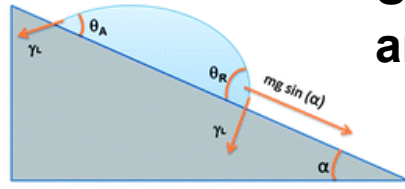
- Corrosion protection
- Self-cleaning coatings
- Anti-icing coating

CONCLUSIONS

Self-cleaning effect

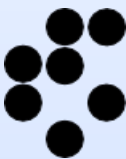


Sliding angle



Water contact angle on rough surface using Wenzel and Cassie–Baxter equation.

Two-step process



MOTIVATION

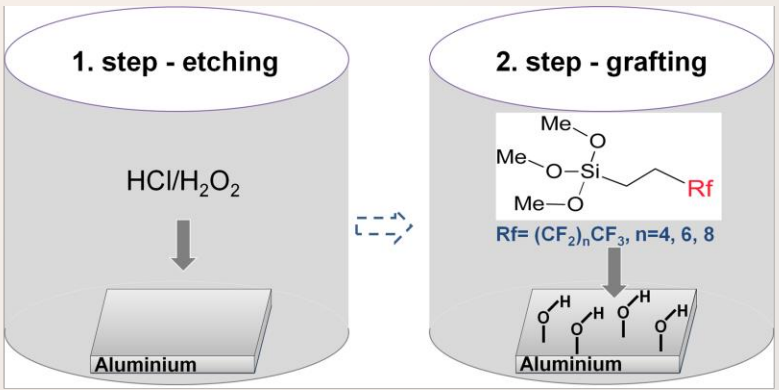
THEORY

PREPARATION

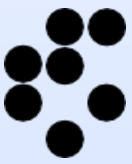
RESULTS

- Corrosion protection
- Self-cleaning coating
- Anti-icing coating

CONCLUSIONS



Scheme 1: Two-step preparation of the superhydrophobic aluminium surface.



Surface analysis

MOTIVATION

THEORY

PREPARATION

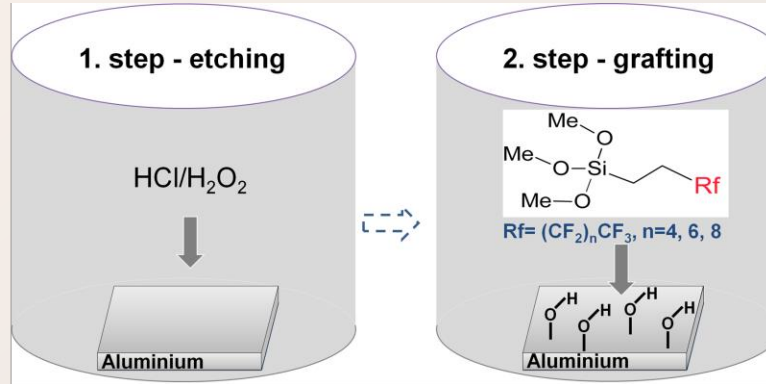
RESULTS

- Corrosion protection

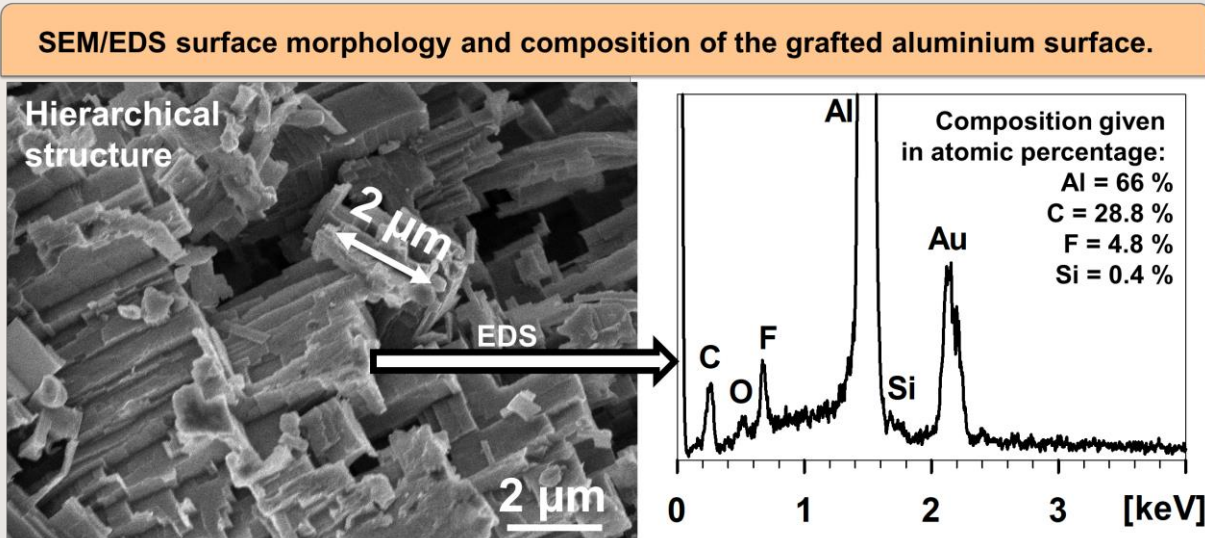
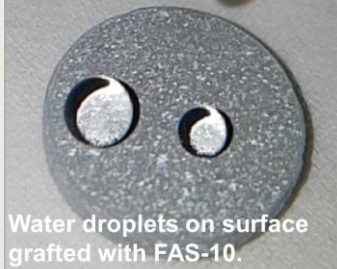
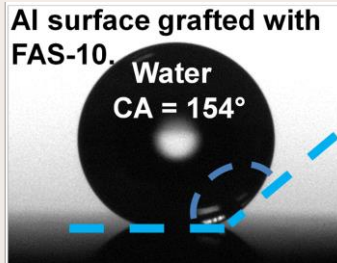
- Self-cleaning coating

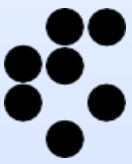
- Anti-icing coating

CONCLUSIONS



Scheme 1: Two-step preparation of the superhydrophobic aluminium surface.





Testing in the corrosive environment

MOTIVATION

THEORY

PREPARATION

RESULTS

- Corrosion protection

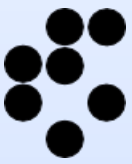
- Self-cleaning coating

- Anti-icing coating

CONCLUSIONS

The surface appearance of ground and treated aluminium surface after various exposure times in the salt spray chamber, according to standard ASTM B117.





Self-cleaning ability

MOTIVATION

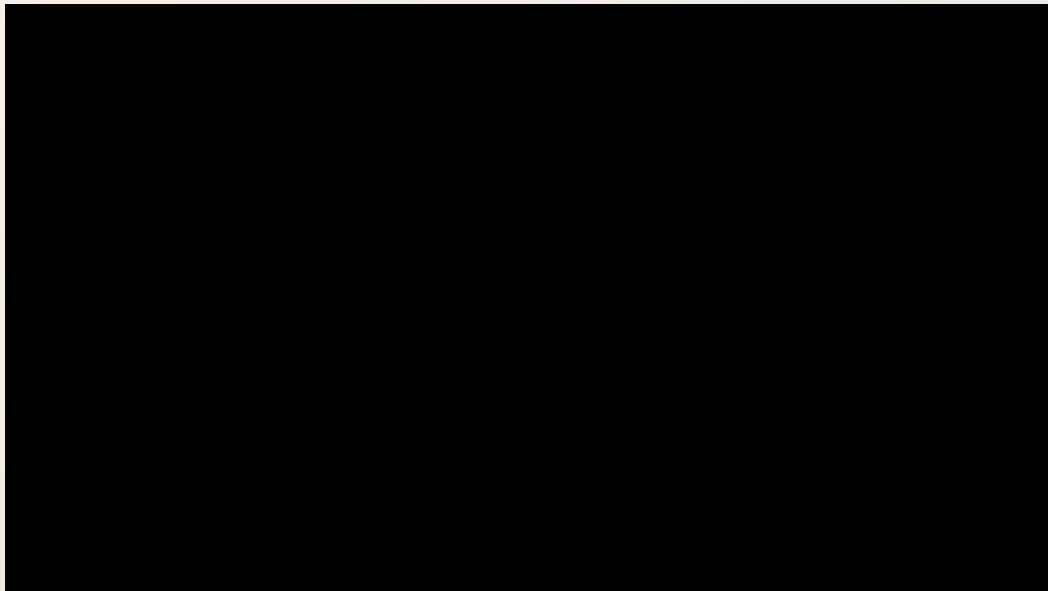
THEORY

PREPARATION

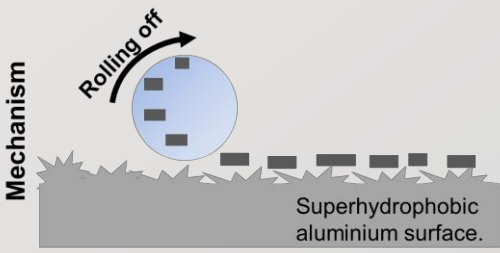
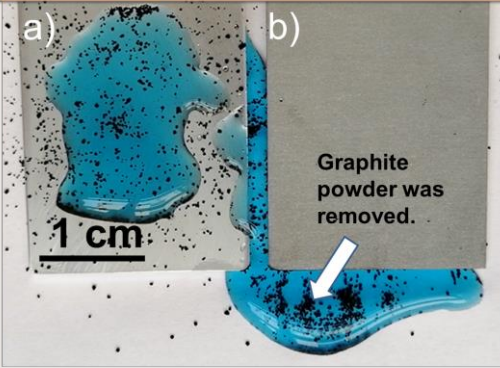
RESULTS

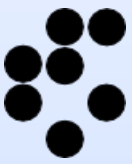
- Corrosion protection
- Self-cleaning coating
- Anti-icing coating

CONCLUSIONS



The self-cleaning ability of a) ground and b) grafted aluminium with FAS-10 coated with graphite powder. The water is coloured with blue dye.





Freezing/melting delay

MOTIVATION

THEORY

PREPARATION

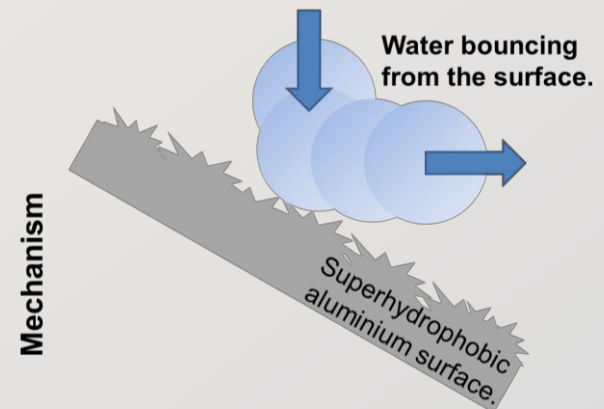
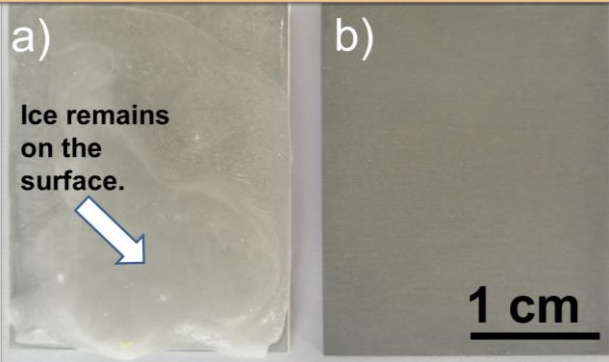
RESULTS

- Corrosion protection
- Self-cleaning coating
- **Anti-icing coating**

CONCLUSIONS



Anti-icing properties of a) ground and b) grafted aluminium with FAS-10. Samples were cooled to $-20\text{ }^{\circ}\text{C}$. Water droplet was dropped on the surface.



Conclusions

MOTIVATION

THEORY

PREPARATION

RESULTS

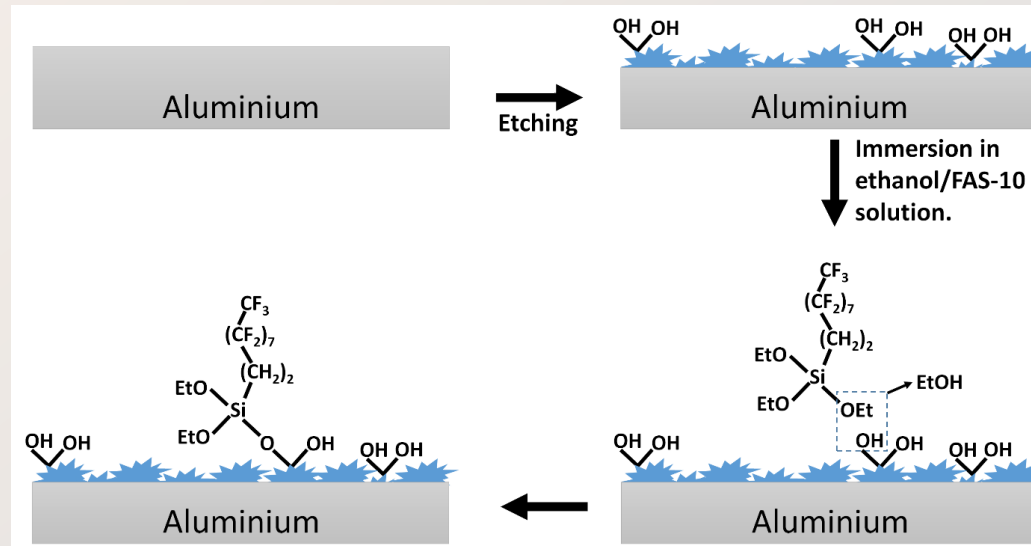
- Corrosion protection
- Self-cleaning coating
- Anti-icing coating

CONCLUSIONS

Such surface treatment:

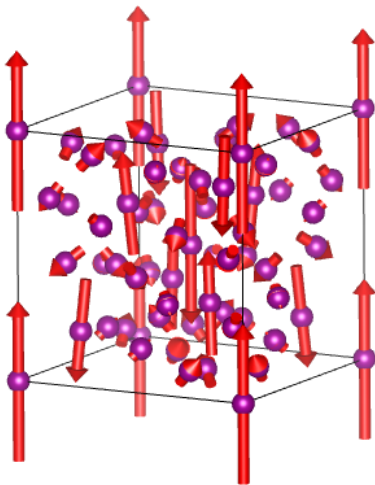
- ✓ enhance corrosion protection,
- ✓ improves self-cleaning ability
- ✓ and gives anti-icing properties.

Mechanism?



It will be continued...with molecular modelling.

Can you guess which material is this?



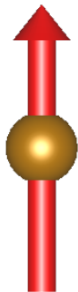
Let's make it simple



LS up



LS down



HS up



HS down

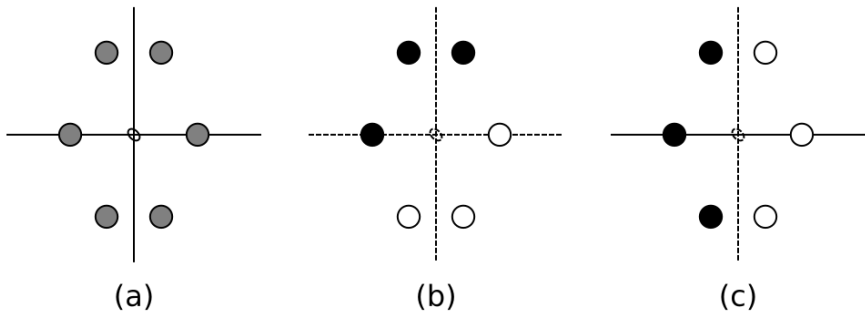


Figure: (a) The original unit cell. (b) A low symmetric choice of spin up and spin down atoms. (c) A highly symmetric choice of spin up and spin down atoms.

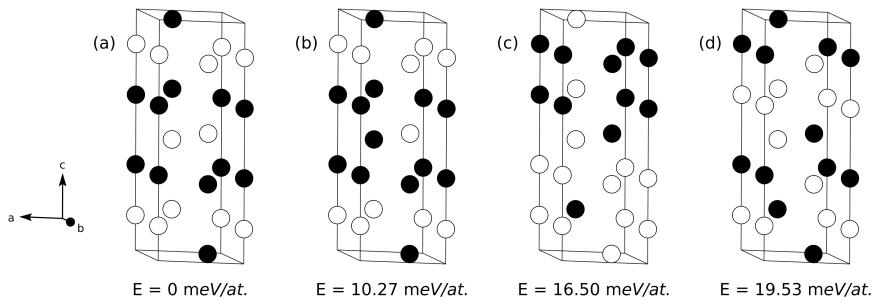


Figure: The four most stable magnetic configurations of hematite after the USPEX run. Energies are expressed with respect to the ground state.

Thank you for your attention!

Are you tired of this?



What about a battery with such a large capacity in your pocket ?



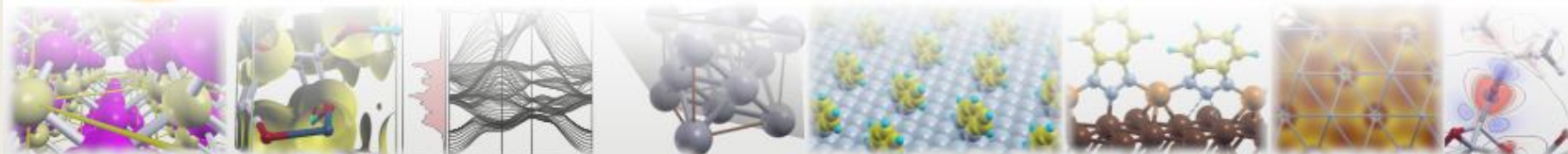


QUANTUMESPRESSO

September 16–20, 2019

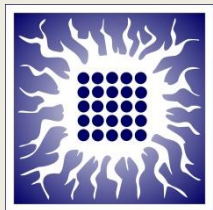
Ljubljana, Slovenia

Summer School on Advanced Materials and Molecular Modelling



Understanding trends in lithium binding at two-dimensional materials

S. Stavrić, Z. S. Popović, Ž. Šljivančanin



Vinča
Institute

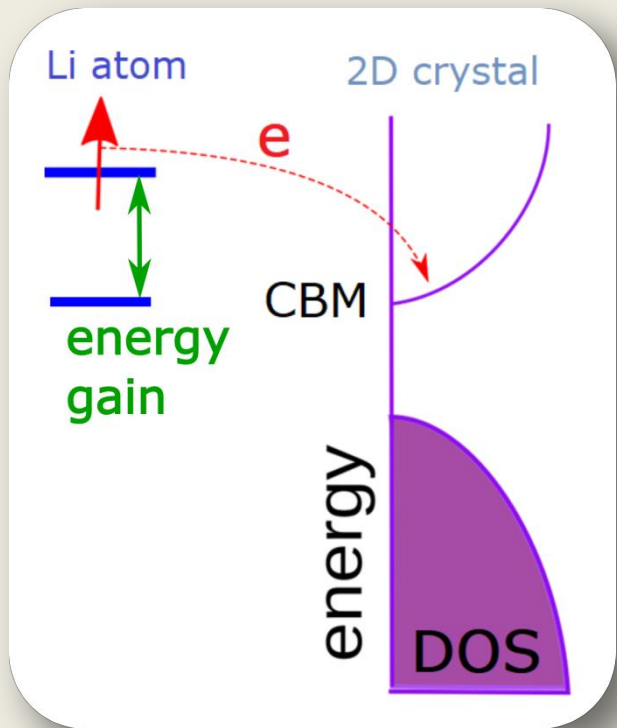
Vinča Institute of Nuclear Sciences,
University of Belgrade,
Serbia

poster no.

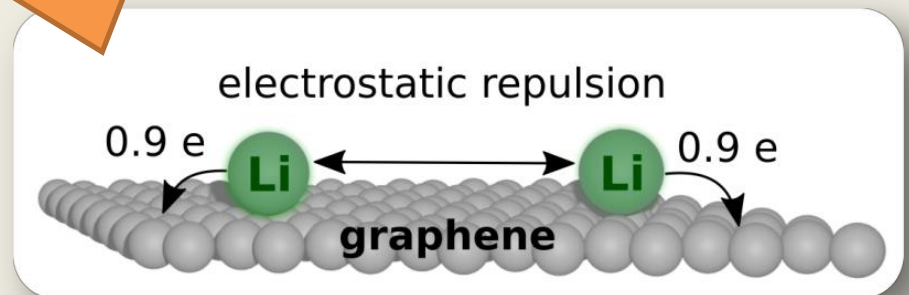
13



1. use 2D materials in electrodes to increase the effective surface ...
2. ... and increase the number of Li adatoms (ions) on the surface

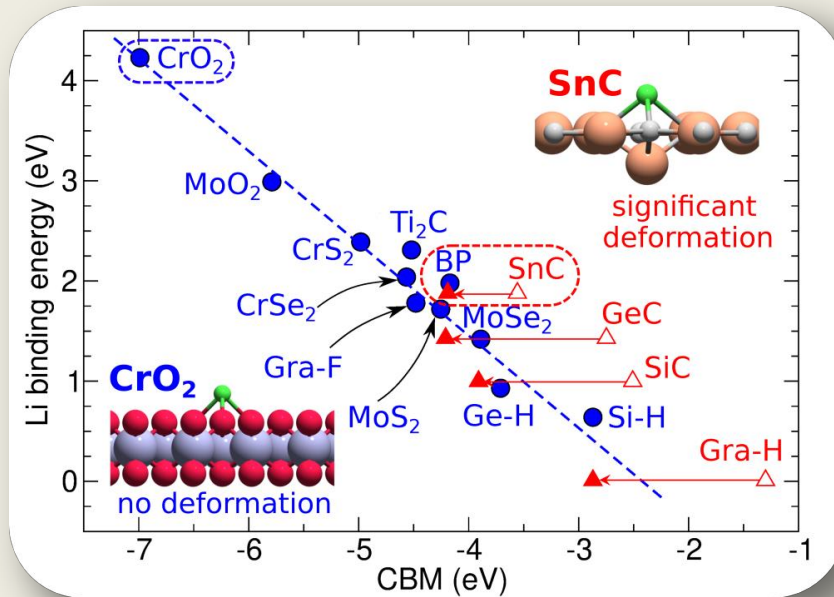


but this will increase the unfavorable electrostatic repulsion between Li adatoms, right?



Not for all 2D materials!

- some 2D materials can localize the electron gained from Li adsorption around the Li atom and thus reduce the unfavorable Li-Li repulsion



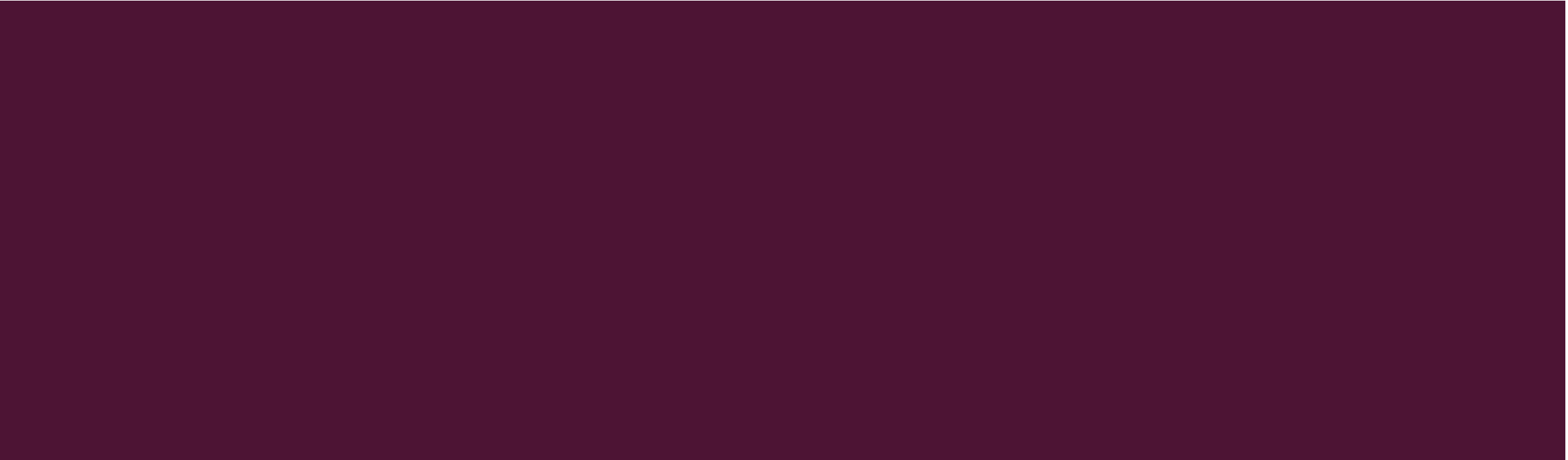
- 15 studied 2D crystals from different families
- 2 characteristic behaviors upon the Li adsorption – two classes of materials

to find out more visit my poster
– lucky number 13



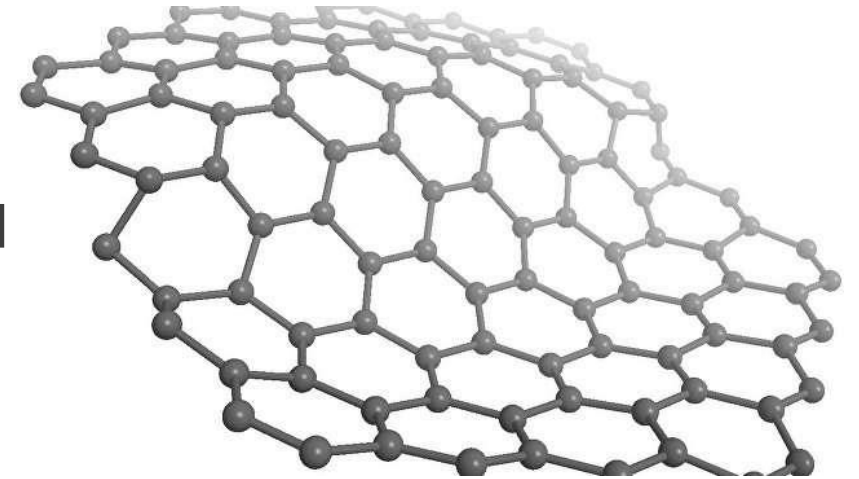
ELECTRON-PHONON INTERACTION AND SUPERCONDUCTIVITY IN GRAPHENE DOPED WITH METAL ATOMS

ANDRIJANA ŠOLAJIĆ, JELENA PEŠIĆ
INSTITUTE OF PHYSICS BELGRADE, SERBIA



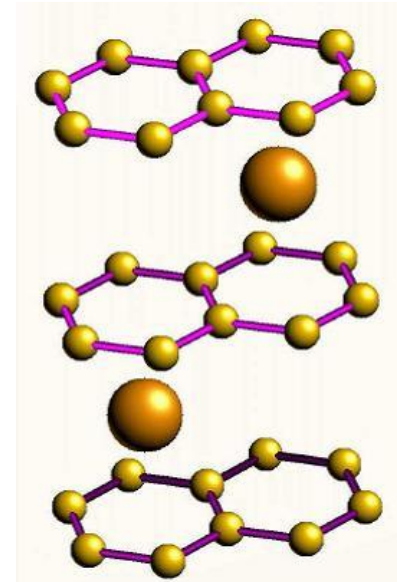
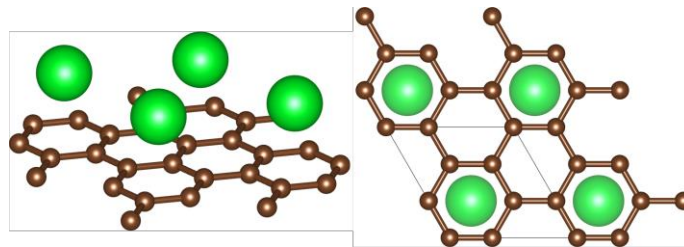
GRAPHENE

- Graphene – material with extraordinary electrical and mechanical properties with plenty of effects and rich physics
- Tuning of properties by various types of defects, applied strain, electrical or magnetic fields..
- One special effect is absent – the superconductivity
- Can we make the graphene superconducting?

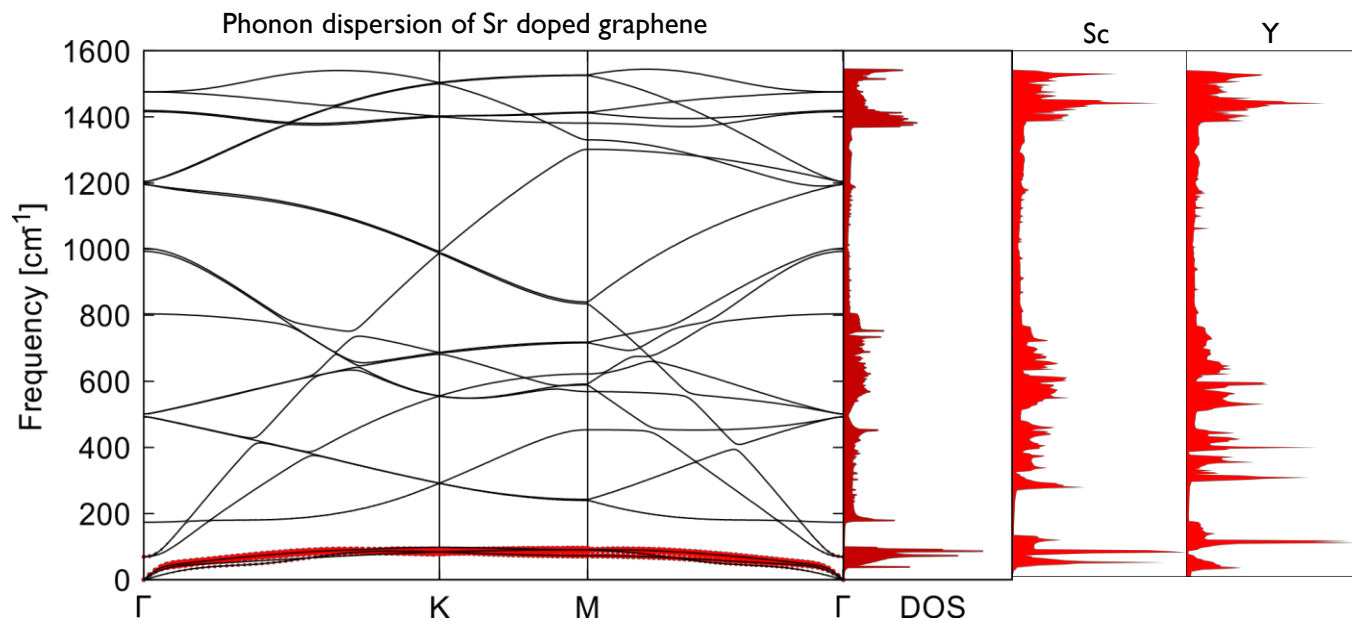


FROM GRAPHITE INTERCALATION COMPOUNDS TO DOPED GRAPHENE

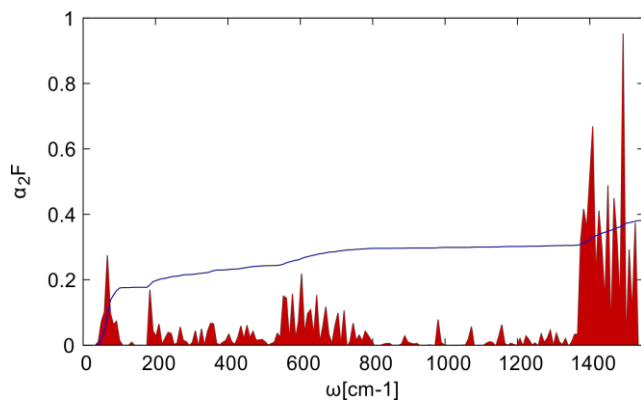
- The old idea – graphite intercalation compounds
- Intercalation of graphite with alkali atoms \rightarrow superconductivity!
- Can we achieve it in a monolayer graphene?
- LiC_6 , CaC_6 with $T_c = 8.1\text{K}$ and 1.5K
- What about the other elements?
- Doping with Sr, Sc and Y



Doping with Sr, Sc and Y

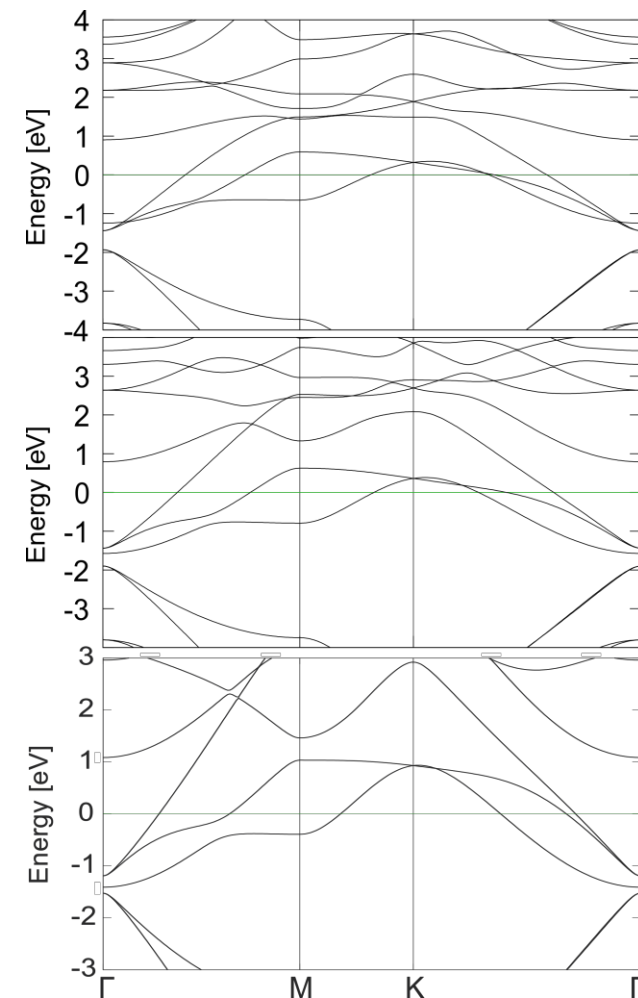


Eliashberg function of Sr doped graphene with electron-phonon coupling parameter in blue line



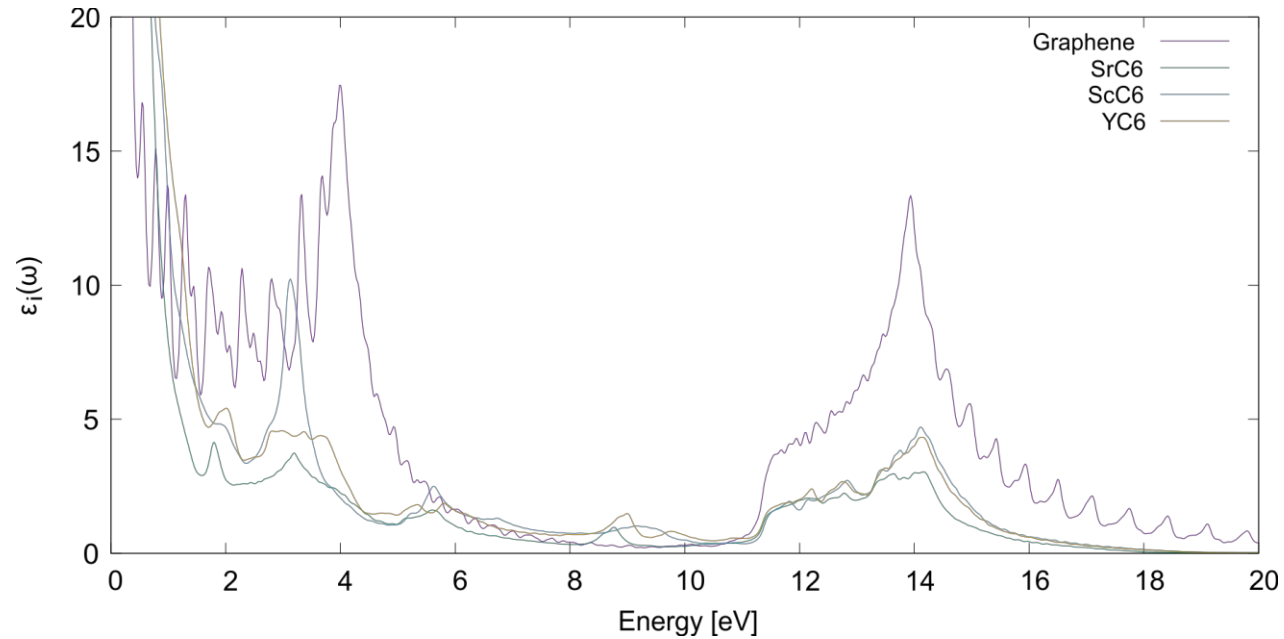
SrC₆
 $\lambda = 0.38$
 $T_c = 0.9K$

$\lambda \approx 0.5$ for YC₆
 $\lambda \approx 0.6$ for ScC₆



Bandstructures of ScS₆, Yc₆ and SrC₆ monolayers, respectively

OPTICAL AND MECHANICAL PROPERTIES



Imaginary part of the dielectric function for pristine graphene and doped graphene structures

	C_{11}	C_{12}	C_{66}	Υ	ν	G
Graphene	462.3	79.6	191.4	225.08	0.19	94.67
ScC6	244.8	37.2	103.8	239.17	0.15	103.83
SrC6	205.9	33.3	86.3	200.46	0.16	86.26
YC6	239.7	38.2	100.8	233.62	0.16	100.77

2nd order elastic constants, Young modulus, Poisson ratio and Shear modulus. All units are in N/m



University of Maribor

Faculty of Chemistry and
Chemical Engineering

Inverse Molecular Docking as a Novel Approach to Study Anticarcinogenic and Anti-neuroinflammatory Effects of Curcumin

Veronika Furlan, Janez Konc, Urban Bren

Ljubljana, september 2019

Curcumin

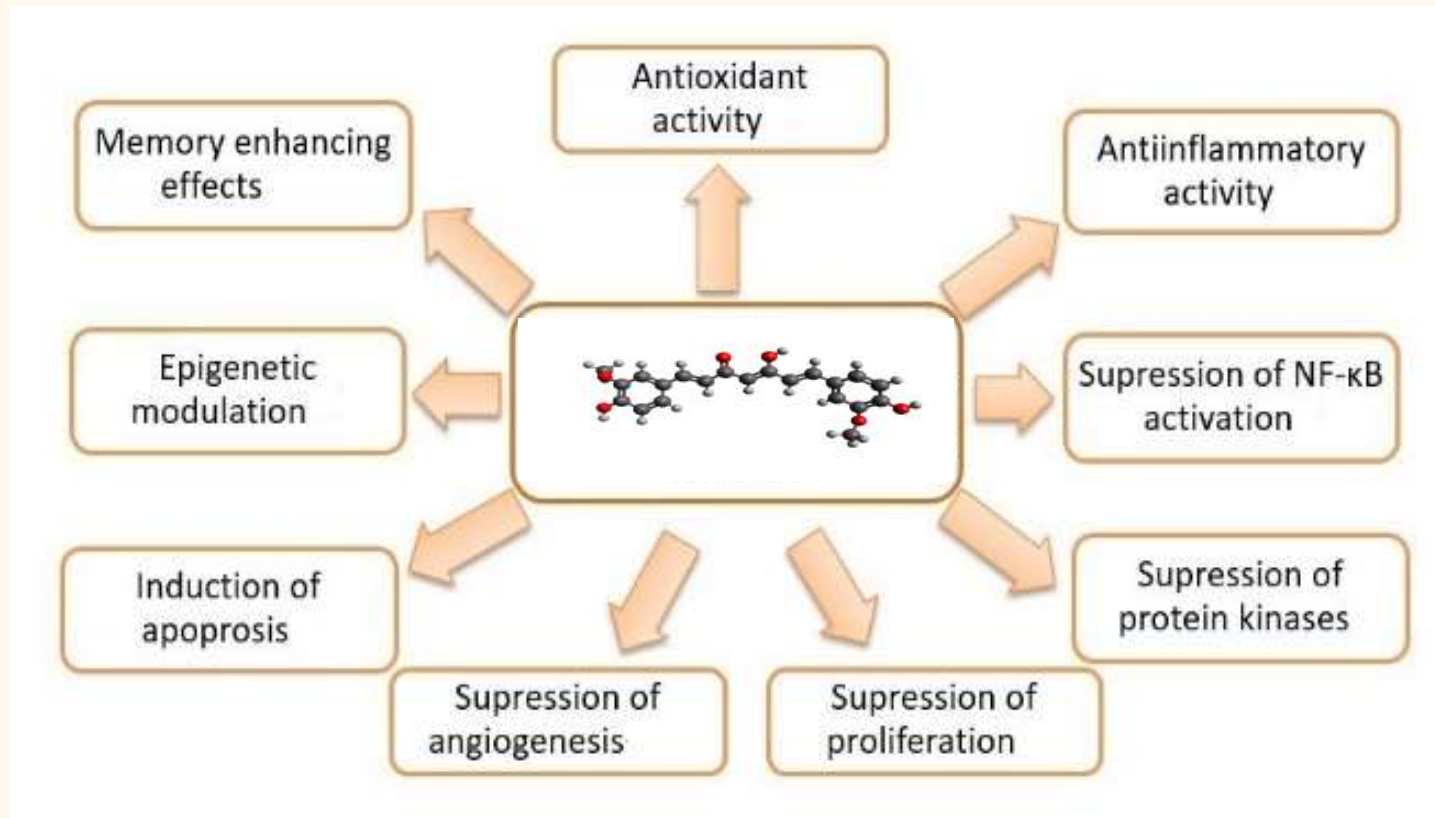


Figure 1: Structural formula and reported biological effects of curcumin.

Computational methods

- Inverse molecular docking:
 - a single small molecule is docked into a collection of protein structures from PDB database.
 - Inverse molecular docking was performed with the novel fragment-based CANDOCK algorithm.
- Inputs to CANDOCK algorithm:
 - ❖ curcumin structure to be inversely docked
 - ❖ human protein chains with their binding sites
- Output:
 - ❖ ranked list of docking score values for minimized protein-curcumin complex structures

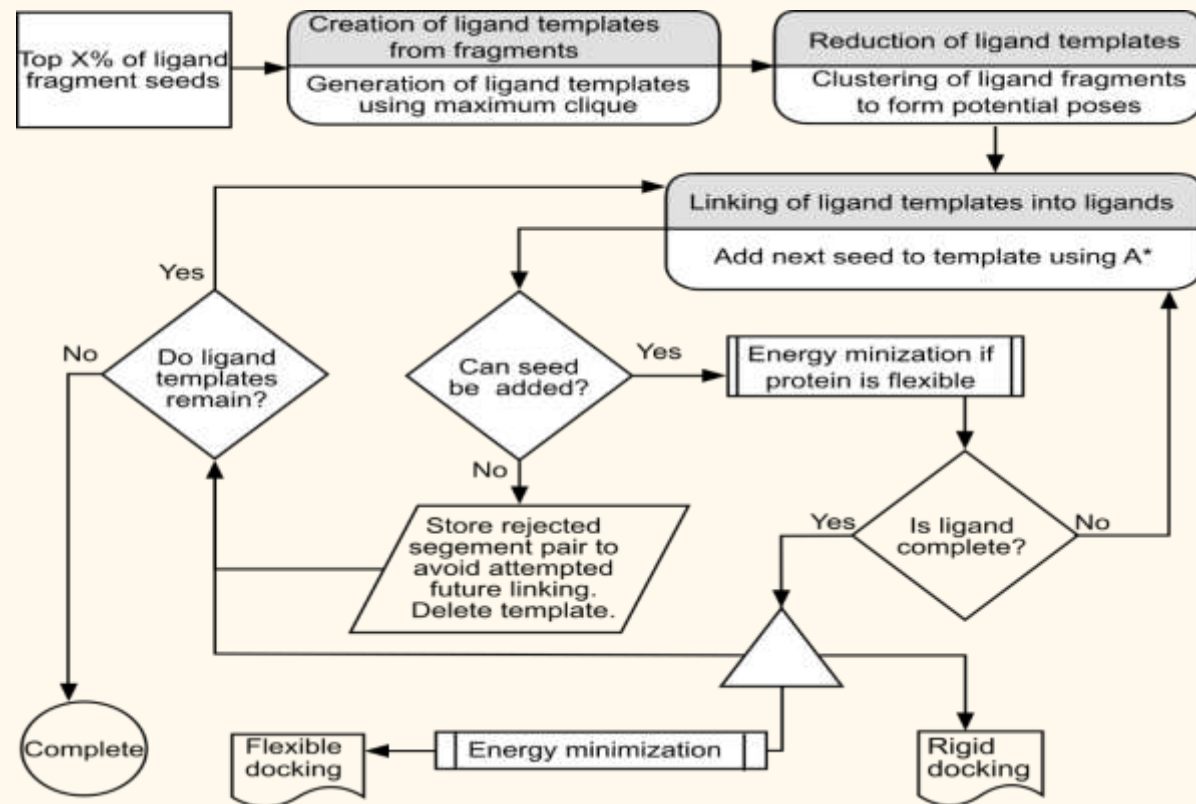
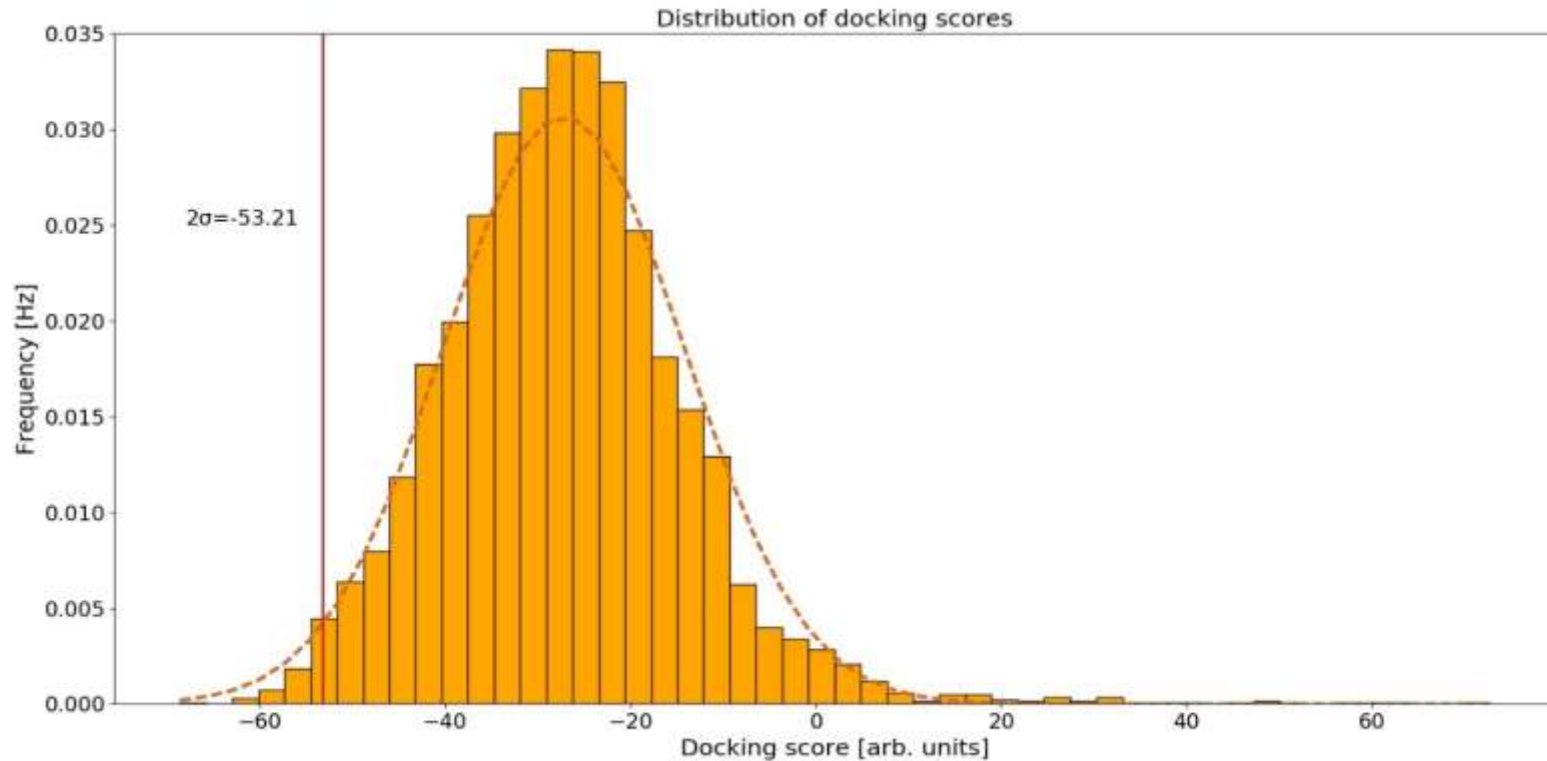


Figure 2: Workflow of the fragment linking procedure.

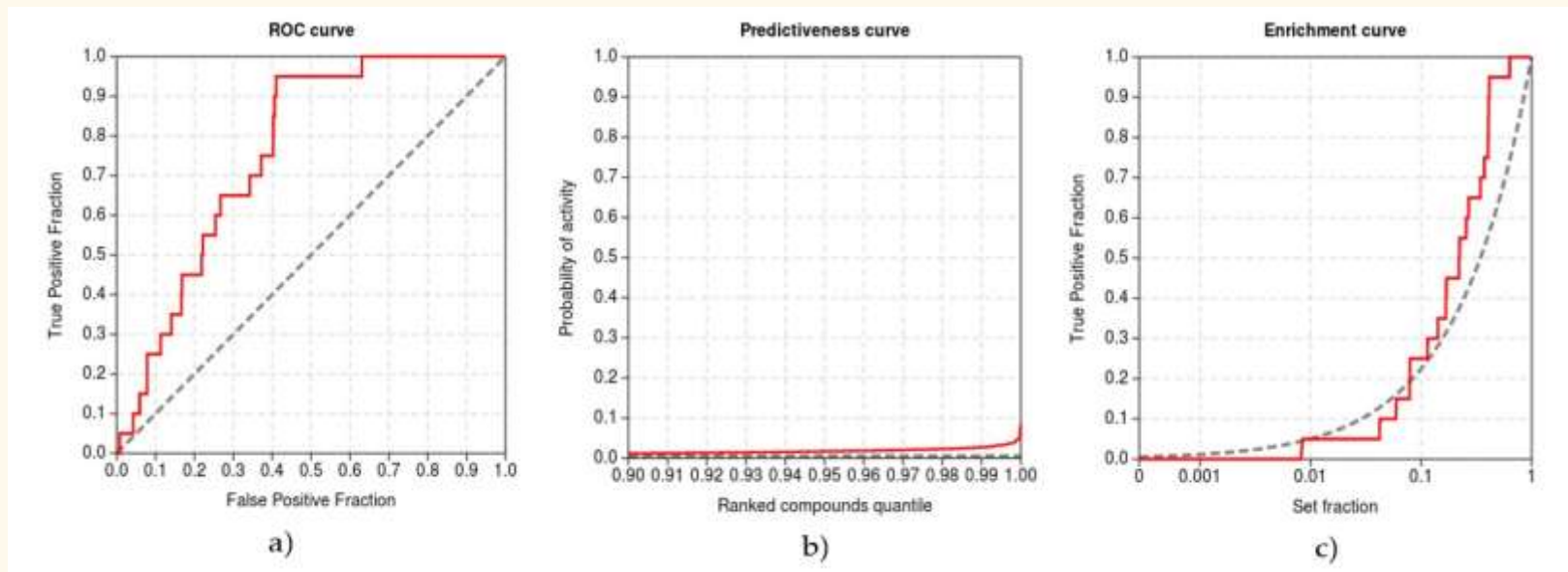
Distribution of Docking Scores



- ❖ 95% confidence interval: $(-53.21, -1.73)$ arb. units
- ❖ Potential curcumin targets \rightarrow proteins with docking scores below -53.21 arb. units (95% confidence interval).

Figure 3: Normal distribution fitting of calculated docking scores.

Validation of the inverse molecular docking protocol



- ❖ ROC AUC = 0.932
 - ❖ BEDROC = 0.370
 - ❖ RIE = 7.288
 - ❖ EF1% = 4.745
 - ❖ TG = 0.684
- Developed protocol is expected to yield a good agreement with experiments.

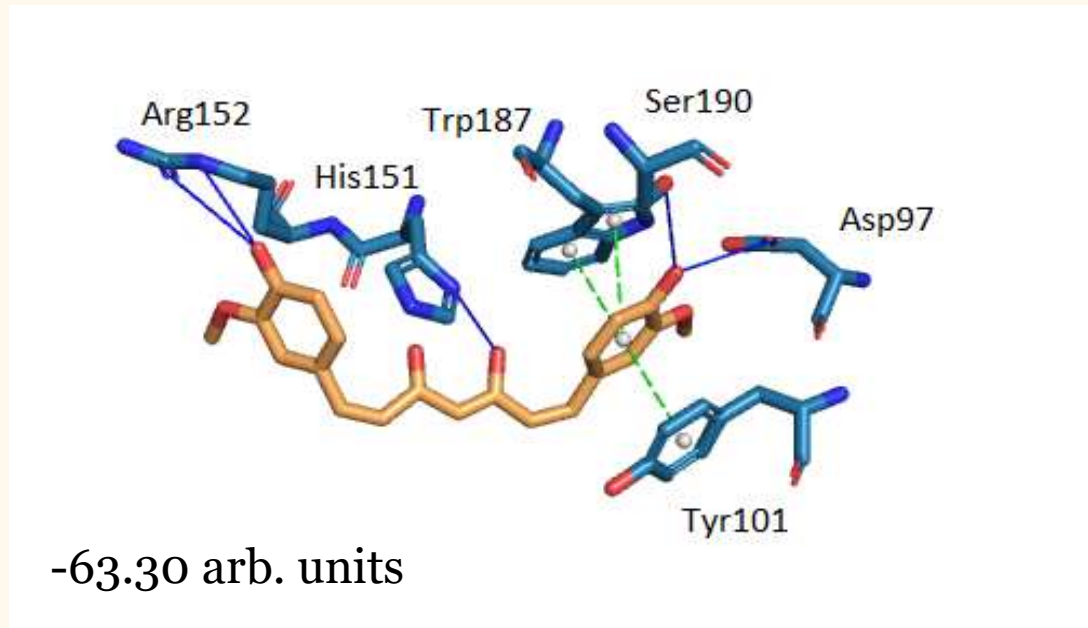
Figure 4: Validation of the inverse molecular docking protocol of curcumin against all human proteins from the Protein Data Bank: a) the ROC curve; b) the predictiveness curve; and c) the enrichment curve.

Identified Protein Targets

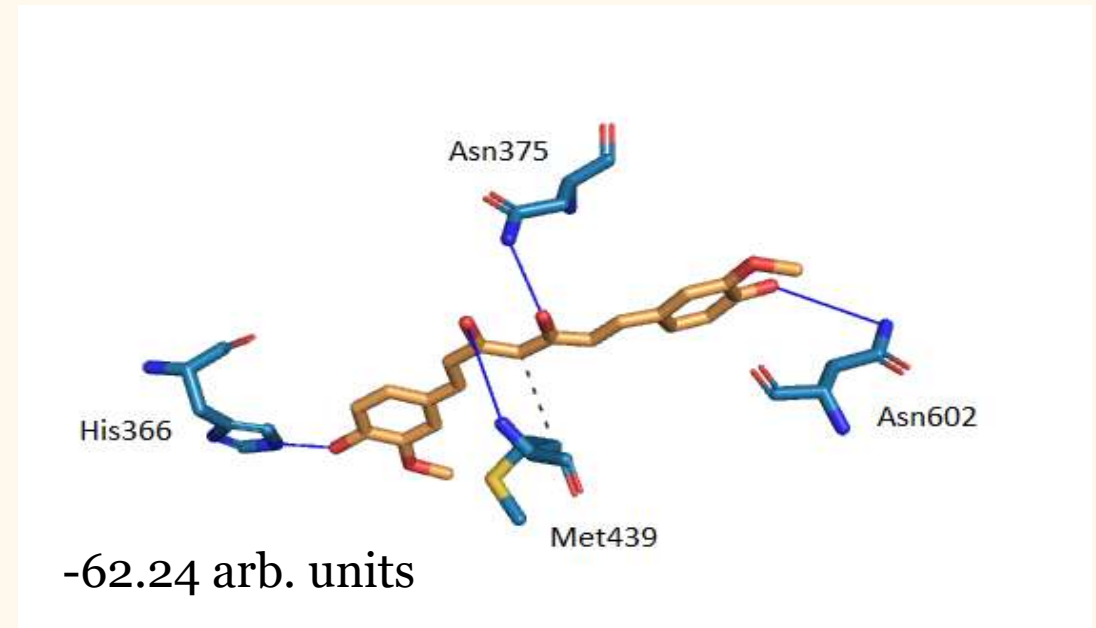
- ❖ We identified 21 potential protein targets of curcumin using the docking score threshold of -53.21 arb. units.
- ❖ Docking scores, functions and reported connections with known diseases are presented in Table 1.

PDB ID with chain	Protein name	Predicted docking scores (arb. units)	Protein function and connections with diseases	Reported experimental correlation with curcumin*
4kmyA	human folate receptor beta (FR- β)	-63.30	Specific delivery of antifolates or folate conjugates to tumors or sites of inflammation.	Yes
3iadA	cAMP-specific 3',5'-cyclic phosphodiesterase 4D (PDE4D)	-62.24	Modulation of cAMP signaling, important in the treatment of Alzheimer's disease, Huntington's disease, schizophrenia, and depression. Interacts with amyloid-beta, connection with neuronal dysfunction associated with Alzheimer's disease.	Yes
1u7tA	17- β -hydroxysteroid dehydrogenase type 10 (17 β -HSD10)	-61.46		No
2qrvA	DNA (cytosine-5)-methyltransferase 3A	-58.59	Regulates methylation of oncogenes.	Yes
1ck7A	metalloproteinase-2 (MMP-2)	-57.93	Regulation of angiogenesis, cell migration, invasion, and formation of metastasis.	Yes
3qeoA	deoxycytidine kinase (dCK)	-57.37	Phosphorylation of deoxyribonucleosides	No
4x3oA	NAD-dependent protein deacetylase sirtuin-2	-56.96	Role in acetylation of histones, regulation of NF- κ B activity.	No
3e7oA	mitogen-activated protein kinase 9 (MAPK-9)	-56.93	Role in cell proliferation, differentiation, cell growth and survival connected to cancer.	Yes
4h2iA	ecto-5'-nucleotidase (e5NT)	-55.95	Role in inflammation, chronic pain, hypoxia, and cancer.	No
4nwgA	tyrosine-protein phosphatase non-receptor type 11	-55.49	Role in cell proliferation.	No
1zr3A	core histone macro-H2A.1	-55.46	Role in acetylation of histones, regulation of NF- κ B activity.	No
4zzjA	NAD-dependent protein deacetylase sirtuin-1	-54.89	Acetylates of histones, regulation of NF- κ B activity and apoptosis.	No
4zseA	epidermal growth factor receptor	-54.81	Regulation of NF- κ B activity.	Yes
5kviA	apoptosis-inducing factor 1 (AP-1)	-54.76	Role in cell proliferation, regulation of apoptosis.	Yes
3lcoA	macrophage colony-stimulating factor 1 receptor (CSF1R)	-54.59	Role in cell proliferation.	No
2rgcA	GTPase HRas	-54.43	Activation of Ras signal transduction pathway.	No
2clpA	aflatoxin B1 aldehyde reductase member 3	-53.86	Protection of liver against the toxic and carcinogenic effects of AFB1.	No
1s1pA	aldo-keto reductase family 1 member C3 (AKR1C3)	-53.69	Role in cell proliferation.	No
3hi7A	amiloride-sensitive amine oxidase	-53.51	Role in cell proliferation, regulation of apoptosis.	No
2a2aA	death-associated protein kinase 2	-53.41	Regulation of apoptosis.	No
1r6tA	tryptophan-tRNA ligase	-53.31	Regulation of angiogenesis.	No

Detailed binding poses of curcumin in the protein targets FR- β and PDE4D with the lowest docking score values



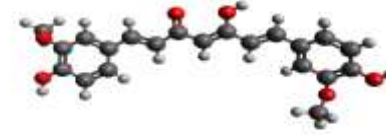
a)



b)

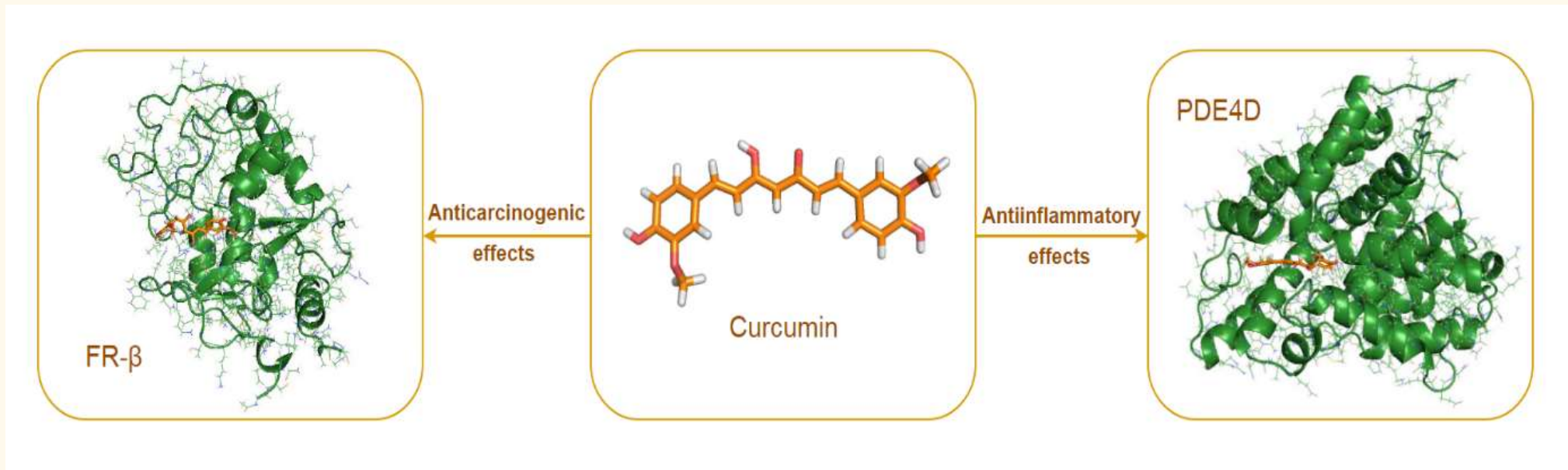
Figure 5: Intermolecular interactions between curcumin and a) the binding site of human folate receptor beta (FR- β), b) the binding site of cAMP-specific 3',5'-cyclic phosphodiesterase 4D (PDE4D). Carbon atoms of curcumin are shown in orange and carbon atoms of amino-acid residues in light blue color. Oxygen atoms are red, nitrogen atoms dark blue and sulfur atoms yellow. Hydrogen bonds are depicted in dark blue. Hydrophobic interaction and pi-stacking interactions are presented with dashed gray and green line, respectively. Hydrogen atoms are omitted for reasons of clarity.

CONCLUSIONS



- We used a novel inverse molecular docking protocol and as the first predicted potential targets of one ligand (curcumin) among all human proteins from the Protein Data Bank.
- The obtained results provide mechanistic insight and can direct future experiments by narrowing down the potential protein targets of curcumin.
- Curcumin potentially binds to proteins playing an important role in:
 - numerous signaling pathways involved in carcinogenesis and tumor formation
 - cognitive impairment associated with Alzheimer's disease.
- A promising opportunity to:
 - identify the most potent analogs of curcumin as well as other natural products and to consequently reduce the associated research costs,
 - identify potential protein targets for new drugs and other chemopreventive compounds originating from various natural sources,
 - predict the potential toxic side-effects of drugs from interactions with proteins other than the targeted one.

Thank you for your attention!



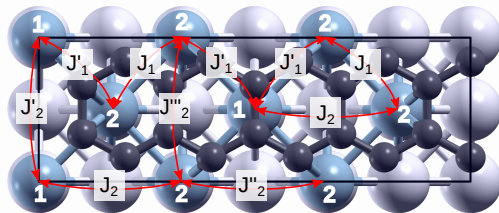
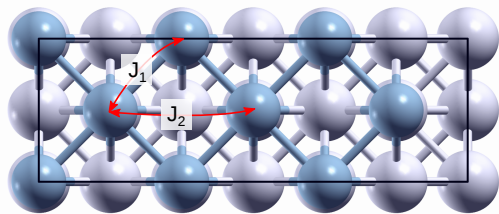
Magnetic interaction of Mn/Cr on Ag(001) surface modified by graphene adsorption

M. Bosnar¹, I. Lončarić¹, P. Lazić¹, I. Žutić², K. D. Belashchenko³

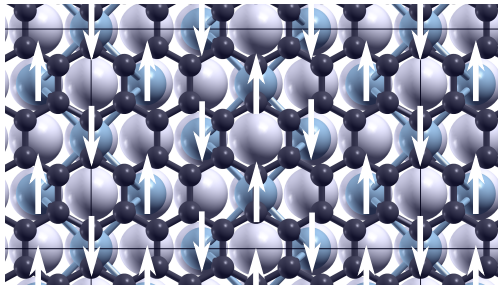
¹ "Ruder Bošković" Institute, Zagreb, Croatia

² University at Buffalo, Buffalo, NY, USA

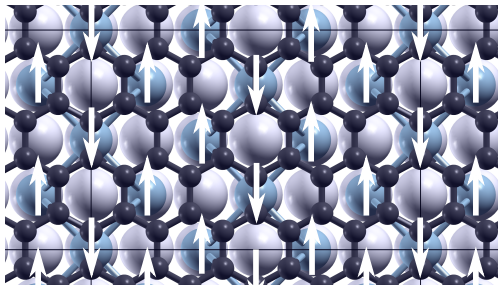
³ University of Nebraska-Lincoln, Nebraska, USA



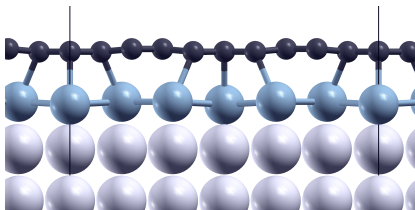
$$E = E_0 - \sum_{i,j} J_{ij} \hat{s}_i \hat{s}_j$$



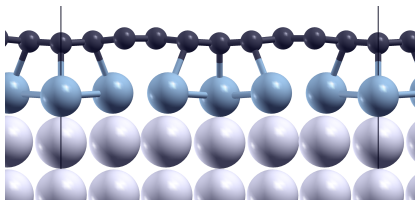
(a) Cr



(b) Mn



(a) Relaxation in ferromagnetic spin configuration



(b) Relaxation in lower symmetry spin configuration

- ▶ Graphene adsorption strongly modifies the magnetic interaction of atoms
- ▶ $+U$ correction results in physisorption of graphene
- ▶ Indications of phonon-magnon coupling

Electron scattering on polaronic impurities characterized by a strong electron-phonon coupling

Juraj Krsnik

Institute of Physics, Zagreb, Republic of Croatia

QE Summer School on Advanced Materials and Molecular Modelling,
18 September 2019

Acknowledgments:



HRZZ

Hrvatska zaklada
za znanost



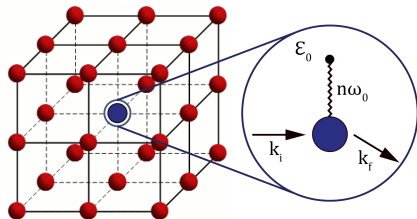
Collaborators:

- Osor Slaven Barišić
- Ivo Batistić
- Eduard Tutiš

INSTITUT ZA FIZIKU

Theoretical model involving polaronic impurity

Scheme of the model:



- polaronic impurity:
 - on-site energy $\varepsilon_0 \neq \varepsilon = 0 \rightarrow$ static impurity
 - coupling between an electron and a local lattice deformation, molecular vibration, ... \rightarrow dynamic impurity
- model Hamiltonian (\mathbf{l} denotes impurity site):

$$\hat{H} = \underbrace{-t \sum_{\langle i,j \rangle} (c_i^\dagger c_j + c_j^\dagger c_i)}_{\hat{H}_0 = \hat{H}_{el} + \hat{H}_{ph}} + \omega_0 a_l^\dagger a_l + \underbrace{\varepsilon_0 c_l^\dagger c_l + g(a_l + a_l^\dagger) c_l^\dagger c_l}_{\text{interaction } \hat{V}}$$

Scattering problem and Green's function formalism

We introduce matrix elements of Green functions

$$G_{\mathbf{n},\mathbf{m}}^{(0)\alpha,\gamma}(\omega) = \langle 0 | \frac{(a_{\mathbf{l}})^{\alpha}}{\sqrt{\alpha!}} c_{\mathbf{n}} \frac{1}{\omega - \hat{H}_0} c_{\mathbf{m}}^{\dagger} \frac{(a_{\mathbf{l}}^{\dagger})^{\gamma}}{\sqrt{\gamma!}} | 0 \rangle = \delta_{\alpha,\gamma} G_{\mathbf{n},\mathbf{m}}^{(0)}(\omega - \alpha\omega_0),$$

$$G_{\mathbf{n},\mathbf{m}}^{\alpha,\gamma}(\omega) = \langle 0 | \frac{(a_{\mathbf{l}})^{\alpha}}{\sqrt{\alpha!}} c_{\mathbf{n}} \frac{1}{\omega - \hat{H}} c_{\mathbf{m}}^{\dagger} \frac{(a_{\mathbf{l}}^{\dagger})^{\gamma}}{\sqrt{\gamma!}} | 0 \rangle,$$

and consider electron scattering on polaronic impurity by using the T-Matrix

$$\hat{T}(\omega) = \hat{V} \hat{G}(\omega) (\omega - \hat{H}_0),$$

where

$$G_{\mathbf{n},\mathbf{m}}^{\alpha,\gamma}(\omega) = \delta_{\alpha,\gamma} G_{\mathbf{n},\mathbf{m}}^{(0)\alpha,\alpha}(\omega) + G_{\mathbf{n},\mathbf{l}}^{(0)\alpha,\alpha}(\omega) T_{\mathbf{l},\mathbf{l}}^{\alpha,\gamma}(\omega) G_{\mathbf{l},\mathbf{m}}^{(0)\gamma,\gamma}(\omega),$$

and

$$\sigma^{\alpha,\gamma}(\varepsilon_{\gamma}) \propto |T_{\mathbf{l},\mathbf{l}}^{\alpha,\gamma}(\varepsilon_{\gamma} + \gamma\omega_0)|^2.$$

Exact solution of the polaronic impurity model

Due to the local interaction $V_{I,I}^{\alpha,\zeta} = \varepsilon_0 \delta_{\alpha,\zeta} + g(\sqrt{\alpha} \delta_{\alpha+1,\zeta} + \sqrt{\zeta} \delta_{\alpha,\zeta-1})$, $T_{I,I}^{\alpha,\gamma}(\omega)$ can be written in a closed form in terms of (there is essential intermediate step - poster!)

$$A_\alpha(\omega) = \frac{g}{\mathcal{G}_{I,I}^{-1}(\omega - (\alpha-1)\omega_0) - \frac{(\alpha-1)g^2}{\mathcal{G}_{I,I}^{-1}(\omega - (\alpha-2)\omega_0) - \frac{(\alpha-2)g^2}{\mathcal{G}_{I,I}^{-1}(\omega - (\alpha-3)\omega_0) - \dots}}} - \text{ph. absorption,}$$

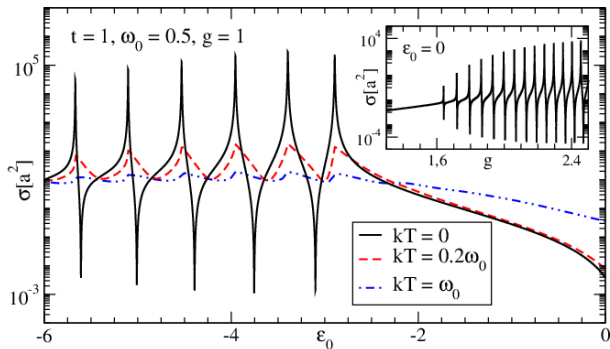
$$B_\alpha(\omega) = \frac{(\alpha+1)g}{\mathcal{G}_{I,I}^{-1}(\omega - (\alpha+1)\omega_0) - \frac{(\alpha+2)g^2}{\mathcal{G}_{I,I}^{-1}(\omega - (\alpha+2)\omega_0) - \frac{(\alpha+3)g^2}{\mathcal{G}_{I,I}^{-1}(\omega - (\alpha+3)\omega_0) - \dots}}} - \text{ph. emission.}$$

→ $T_{I,I}^{\alpha,\gamma}(\omega)$ are known to any order in the perturbation theory and the polaronic impurity problem is fully solved.

Average scattering cross section

$$\sigma(T) = \sum_{\alpha, \gamma} \underbrace{D_\gamma(T)}_{\text{ph. distr.}} \int d\varepsilon_\gamma \underbrace{p(\varepsilon_\gamma, T)}_{\text{el. distr.}} \underbrace{\left[\frac{a^2}{4\pi t^2} \sqrt{\frac{\varepsilon_\alpha}{\varepsilon_\gamma}} |T^{\alpha, \gamma}(\varepsilon_\gamma + \gamma\omega_0)|^2 \right]}_{\sigma^{\alpha, \gamma}(\varepsilon_\gamma)}$$

- exact results for the simple cubic lattice:





DOES SIZE REALLY MATTER?

Density Functional Theory (DFT) and kinetic Monte Carlo (kMC) of RWGS on Cu/SrTiO_3 bifunctional catalysts

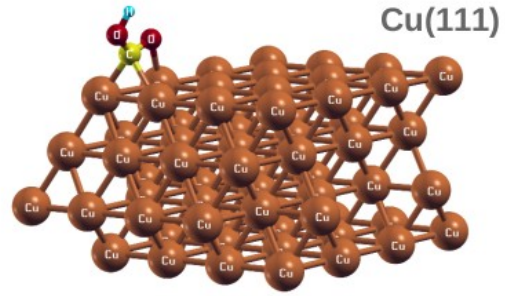
Drejc Kopač, Matej Huš, Blaž Likozar

Department of Catalysis and Chemical Reaction Engineering, National Institute of Chemistry, Ljubljana, Slovenia

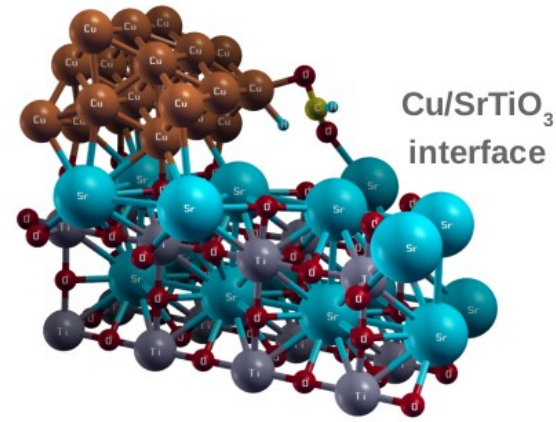
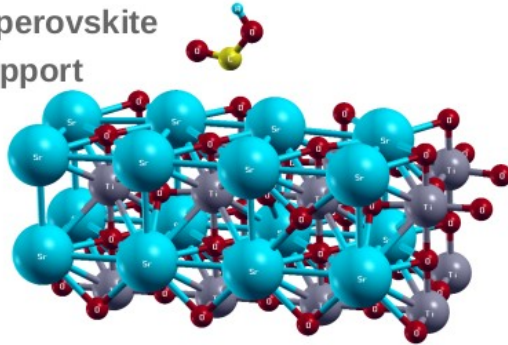


METHODS

- **DFT**: - structure optimization, pathway energetics, pairwise interactions, transition states
 - PAW pseudopotentials, gradient-corrected PBE exchange correlation
 - 450 eV kinetic energy cut-off, Grimme D3 correction

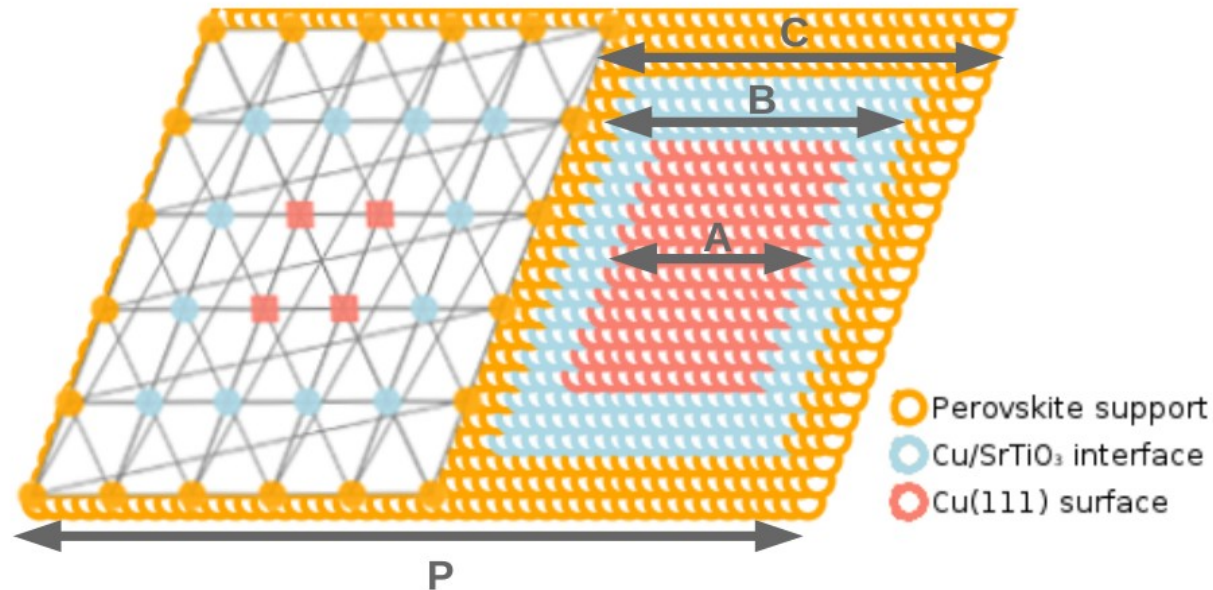


SrTiO₃ perovskite support



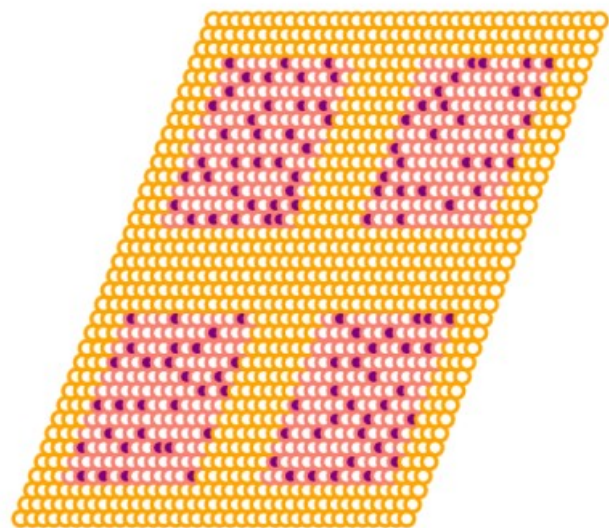
METHODS

- **kMC:** - variable lattice sizes, various temperatures and pressures
 - graph-theoretical kMC algorithm, Zacros software
 - cluster expansion model: pairwise 1st nearest neighbour interactions
 - kinetic constants from TST, E-R and L-H type reactions



RESULTS

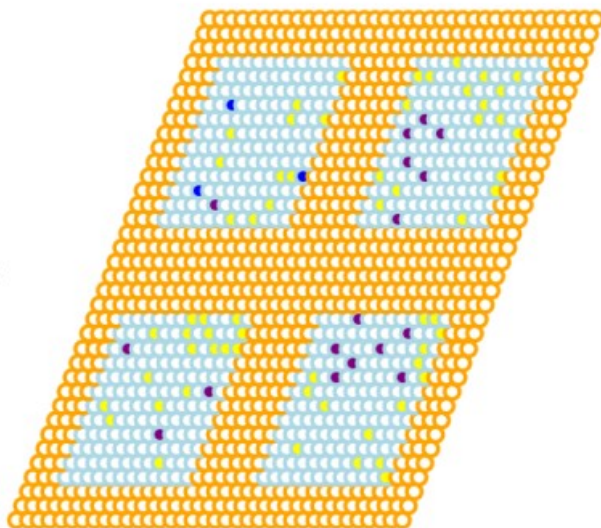
Bifunctional catalyst is more active



Cu + support

$$\text{TOF}_{\text{CO}} = 4.3 \times 10^{-7} \text{ s}^{-1}$$

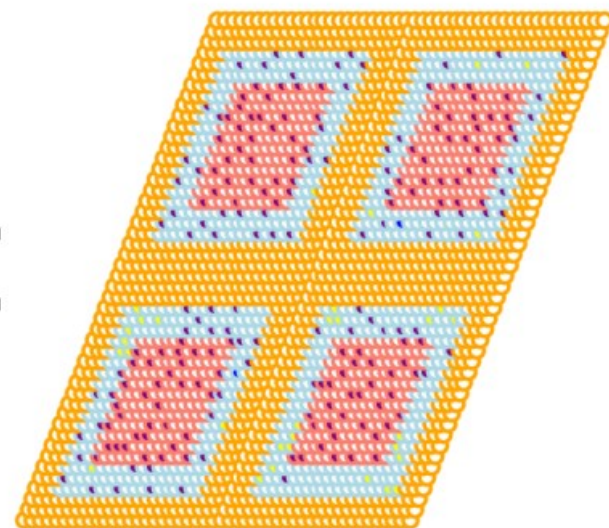
+



Interface + support

$$\text{TOF}_{\text{CO}} = 7.1 \times 10^{-5} \text{ s}^{-1}$$

<

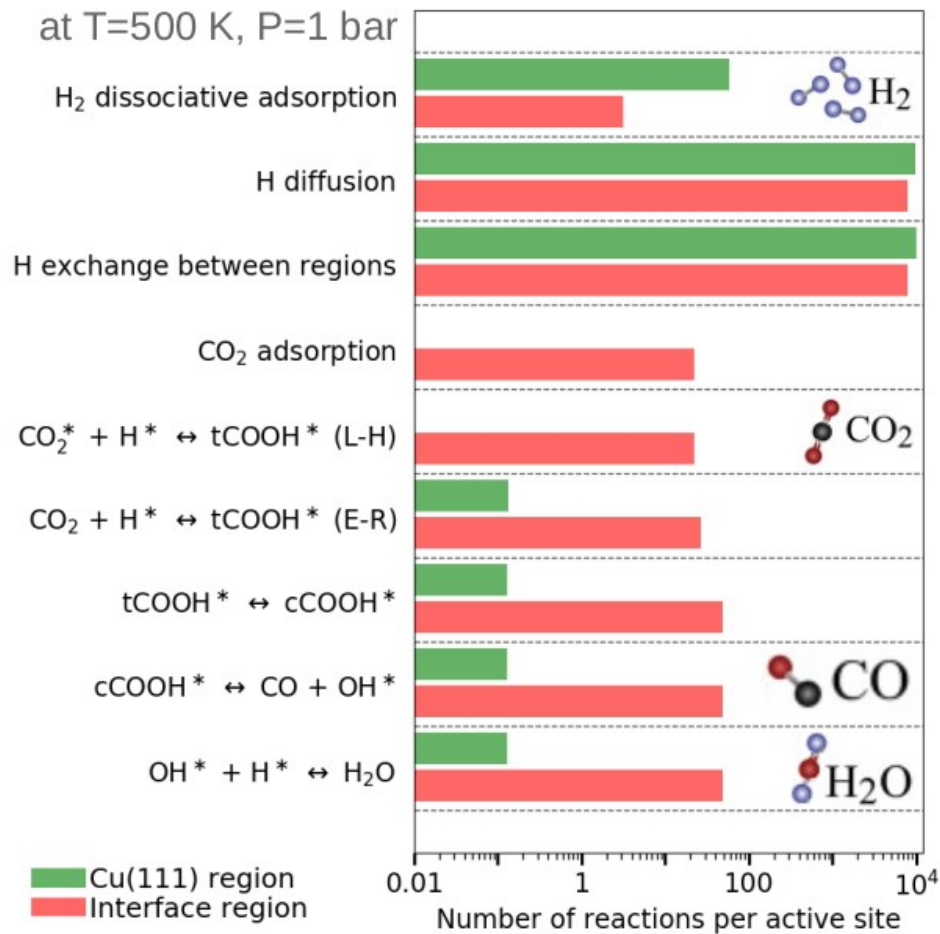


Cu + interface + support

$$\text{TOF}_{\text{CO}} = 9.4 \times 10^{-5} \text{ s}^{-1}$$

CO rate per active site (TOF) shows that bifunctional catalyst is more active for CO production.

RESULTS



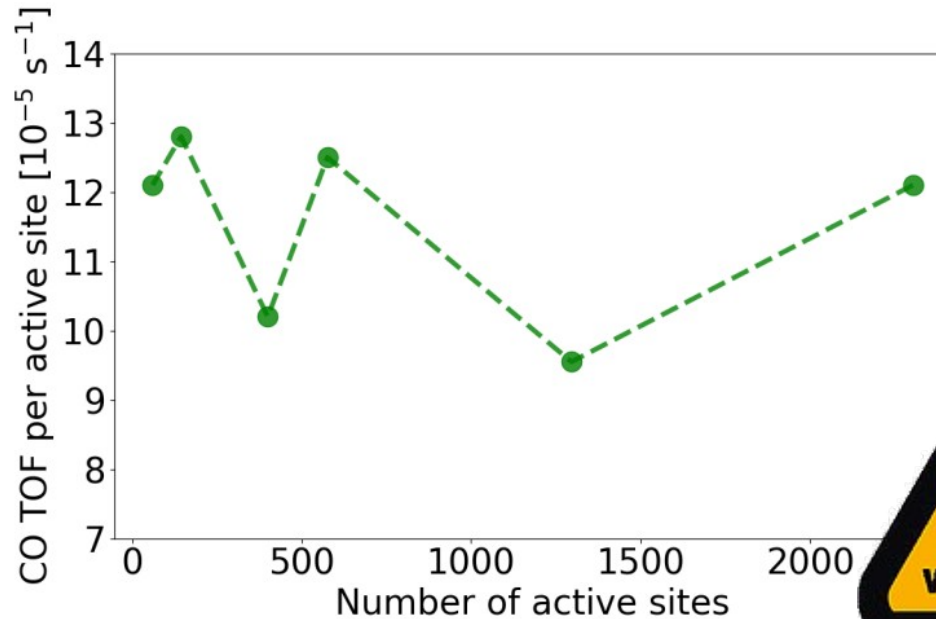
→ Cu(111) superior for H₂ adsorption

→ H diffuses to perovskite interface

→ CO₂ hydrogenation preferred on Cu/SrTiO₃ interface region

No catalytic activity on perovskite support surface!

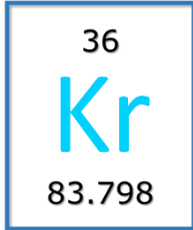
CONCLUSIONS

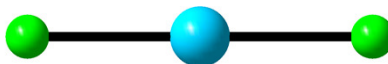


CO TOF vs number of active sites does not show any trends. These are preliminary results, more thorough simulations are in progress.

- **Activity (TOF) towards CO is improved when using bifunctional catalyst.**
- **Preliminary results show no clear trend when comparing the catalytic activity and size.**

Probing the fluoride ion donor

properties of  F_2



Matic Lozinšek,^{1,2,3} Hélène P. A. Mercier,¹ Gary J. Schrobilgen¹

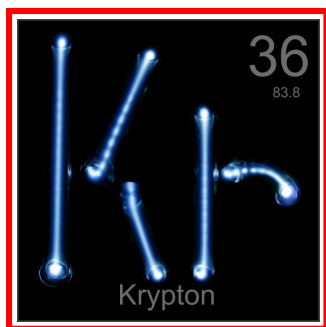
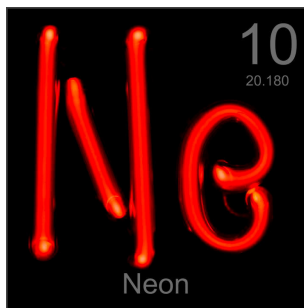
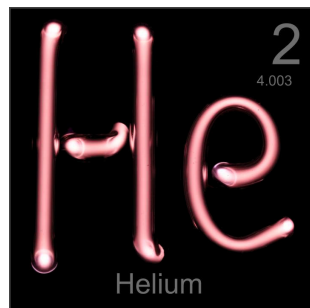
¹ *Department of Chemistry, McMaster University, Hamilton, ON, Canada*

² *Department of Inorganic Chemistry and Technology, Jožef Stefan Institute, Ljubljana, Slovenia*

³ *Faculty of Chemistry and Chemical Technology, University of Ljubljana, Ljubljana, Slovenia*

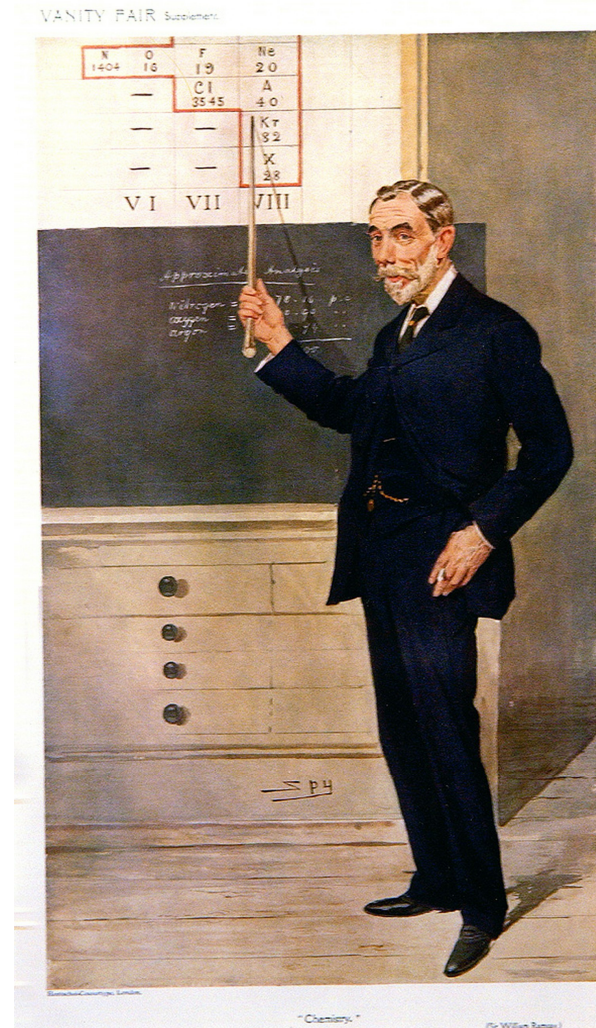
Noble Gases

Group 18 (VIIIa) Elements



<http://www.periodictable.com/>

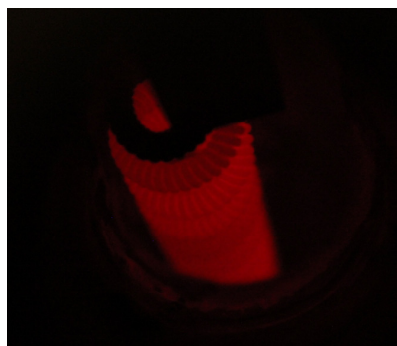
Historically known as the ~~Inert~~ Gases.



Sir William Ramsay
1894 Ar; 1898 Ne, Kr, Xe

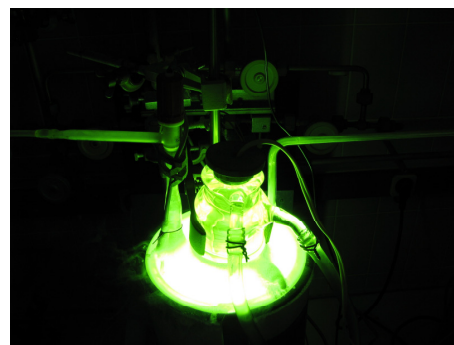
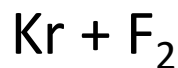
Krypton Chemistry \approx Chemistry of KrF_2

$\Delta H_f = 60.2 \text{ kJ/mol} \Rightarrow$ Thermodynamically unstable! \Rightarrow Better F^\bullet source than F_2 !

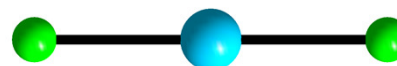
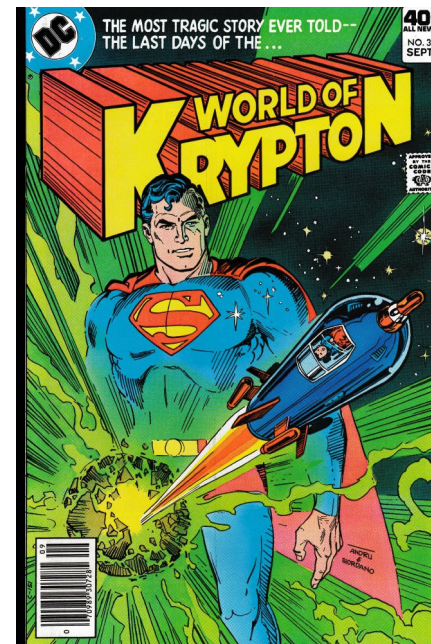


Coiled Ni Filament
(Hot-Wire Reactor)

← Syntheses →



UV Photolysis



J. F. Lehmann, H. P. A. Mercier, G. J. Schrobilgen, *Coord. Chem. Rev.* **2002**, 233–234, 1.

M. Lozinšek, G. J. Schrobilgen, *Nature Chem.* **2016**, 8, 732.

Fluorine Laboratory

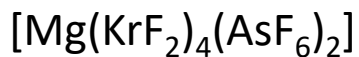
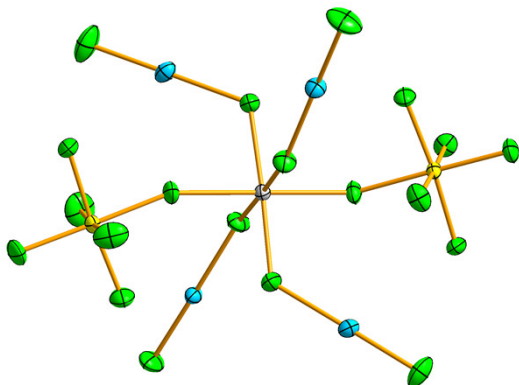


Inspiring Innovation and Discovery

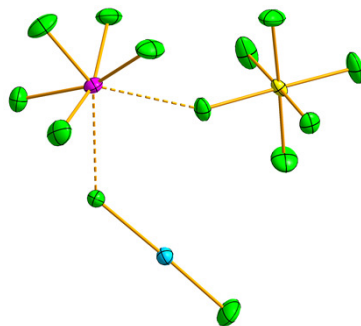


New Kr Compounds

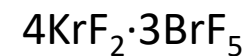
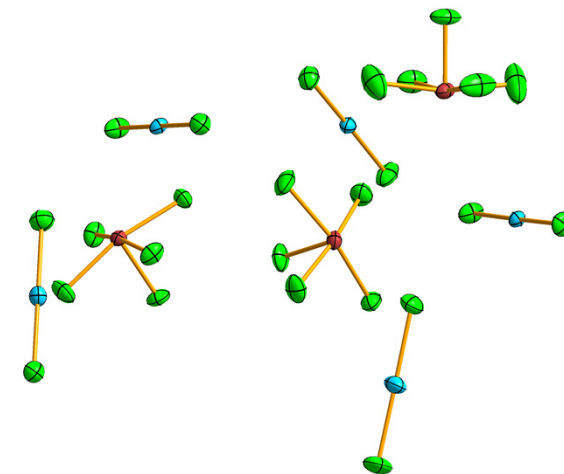
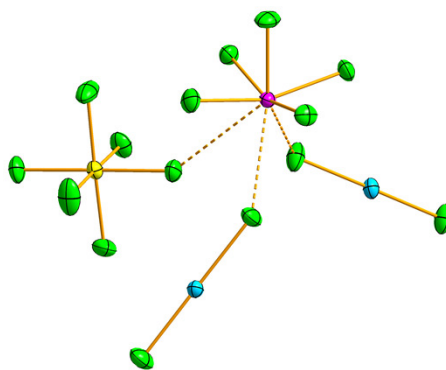
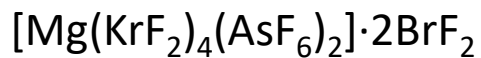
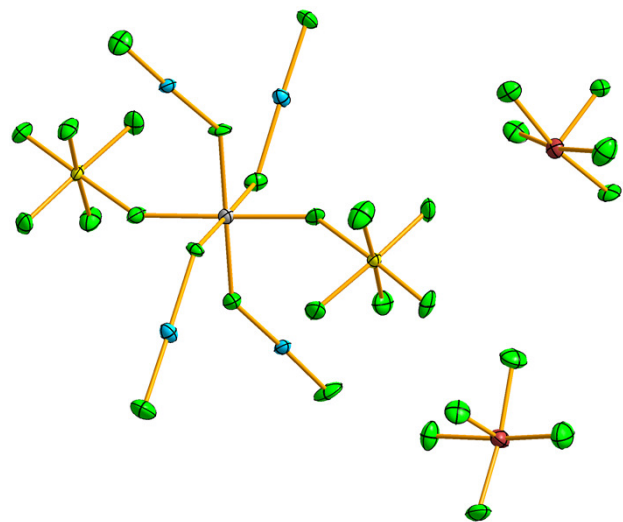
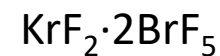
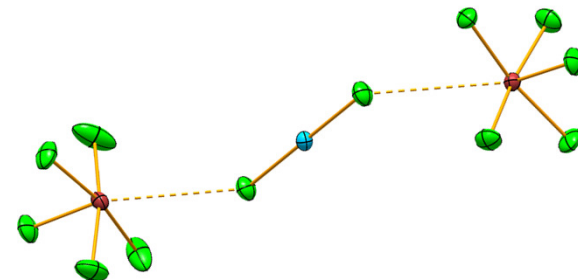
Mg²⁺-KrF₂ Complex



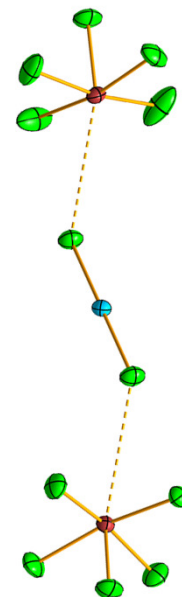
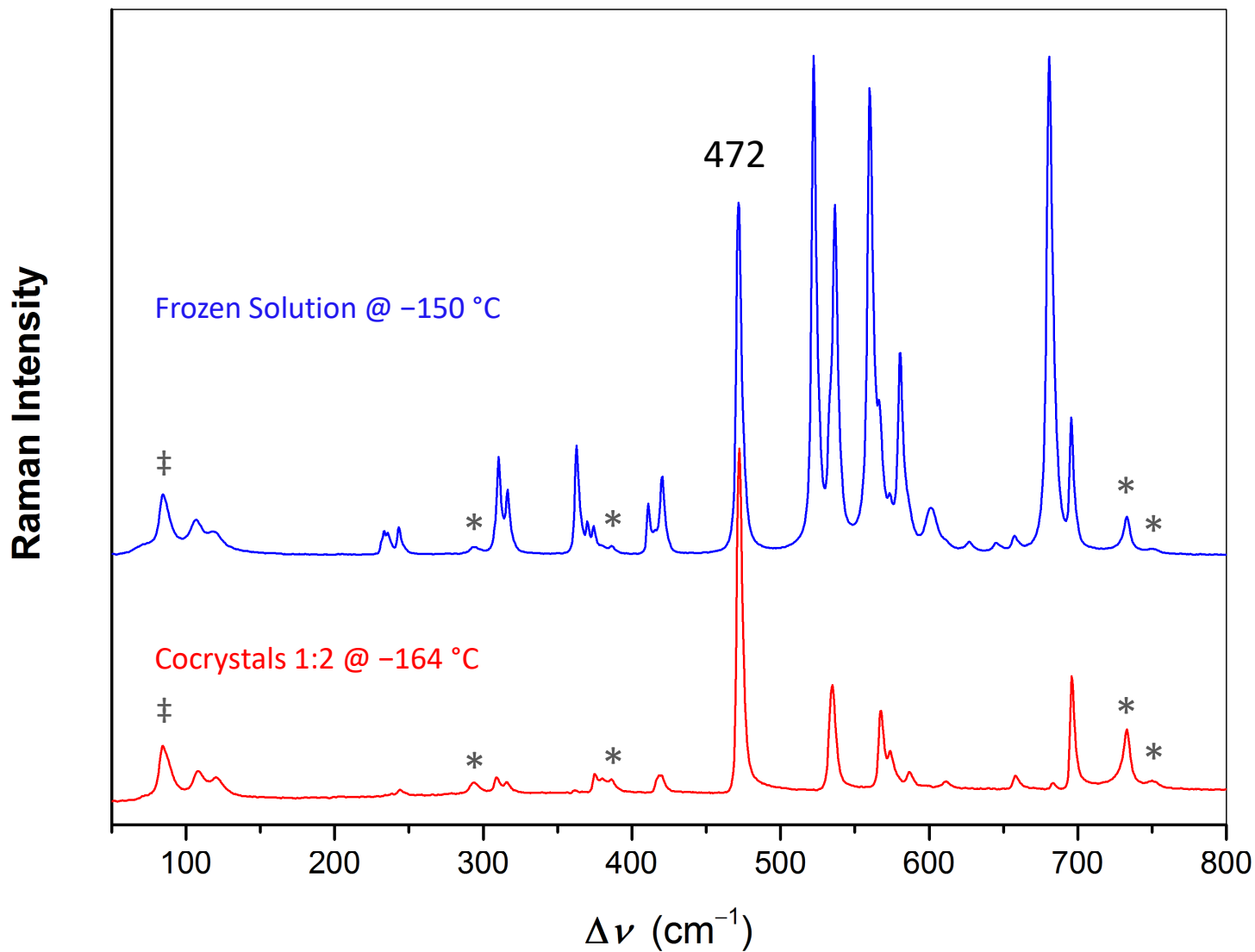
Mixed Xe-Kr Compounds



KrF₂-BrF₅ Co-crystals



KrF₂·2BrF₅



Symbols denote FEP sample tube lines (*), and instrumental artifact (†).



Acknowledgments



Prof. Dr. Gary J. Schrobilgen, *McMaster University*

Dr. H el ene P. A. Mercier, *McMaster University*

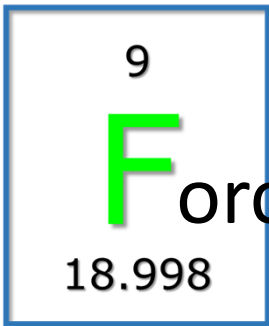
Prof. Dr. Boris  zemva, *Jo ef Stefan Institute*

This research was supported by a

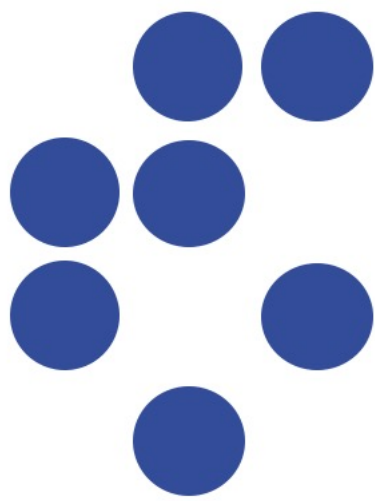
Marie Curie International Outgoing Fellowship

within the

7th European Community Framework Programme.

May the  Force be with you!



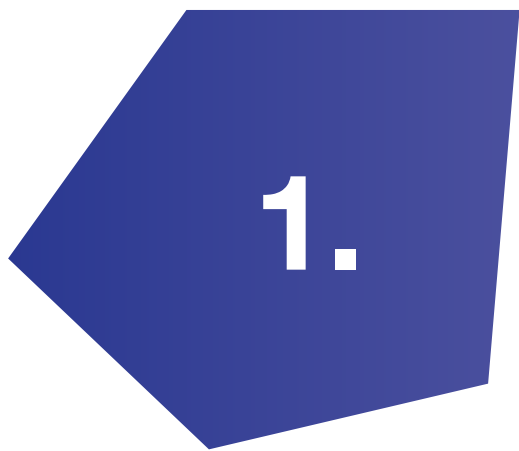


Jožef Stefan Institute

The role of small coadsorbates on adsorption of azole molecules on copper surfaces

Matjaž Dlouhy

Department of Physical and Organic Chemistry



1.

What are we doing?

Modelling corrosion inhibitors on copper surfaces using DFT.

1.

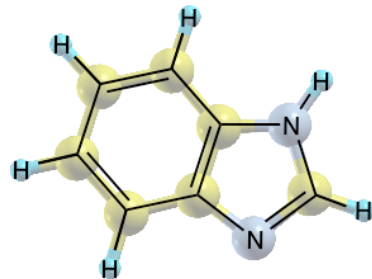
What are we doing?

Modelling **corrosion inhibitors** on copper surfaces using DFT.

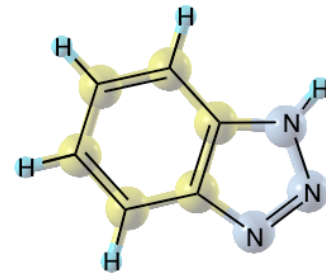
substances with ability to reduce corrosion



imidazole



benzimidazole



benzotriazole

1.

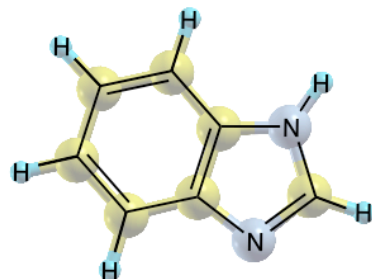
What are we doing?

Modelling corrosion inhibitors on copper surfaces using DFT.

substances with ability to reduce corrosion



imidazole



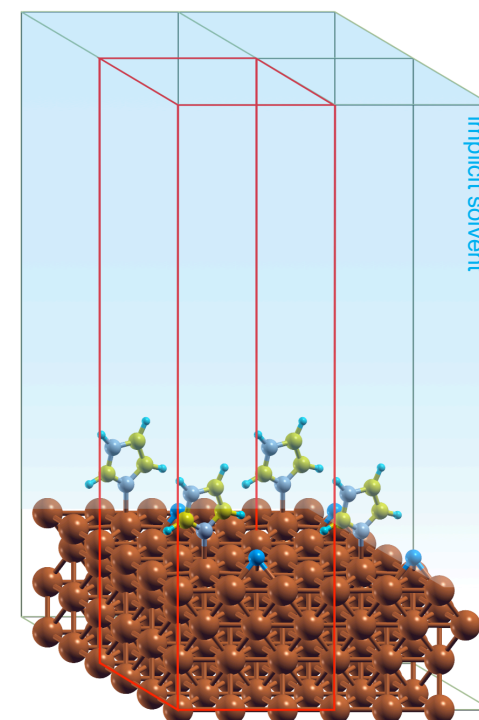
benzimidazole



benzotriazole

periodic multi-slab
model of Cu(111)
surface

XCrySDen



1.

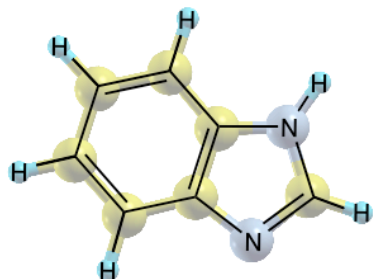
What are we doing?

Modelling corrosion inhibitors on copper surfaces using DFT.

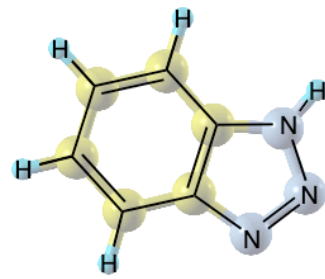
substances with ability to reduce corrosion



imidazole



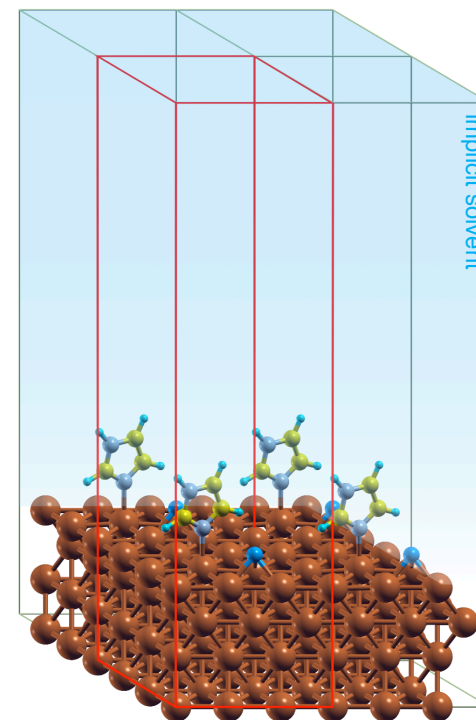
benzimidazole



benzotriazole

periodic multi-slab
model of Cu(111)
surface

XCrySDen



DFT framework
using the (PBE)
energy functional

Environ





Evaluate how some coadsorbed corrosion relevant species affect intermolecular interactions of adsorbed azole molecules.



H



O



OH



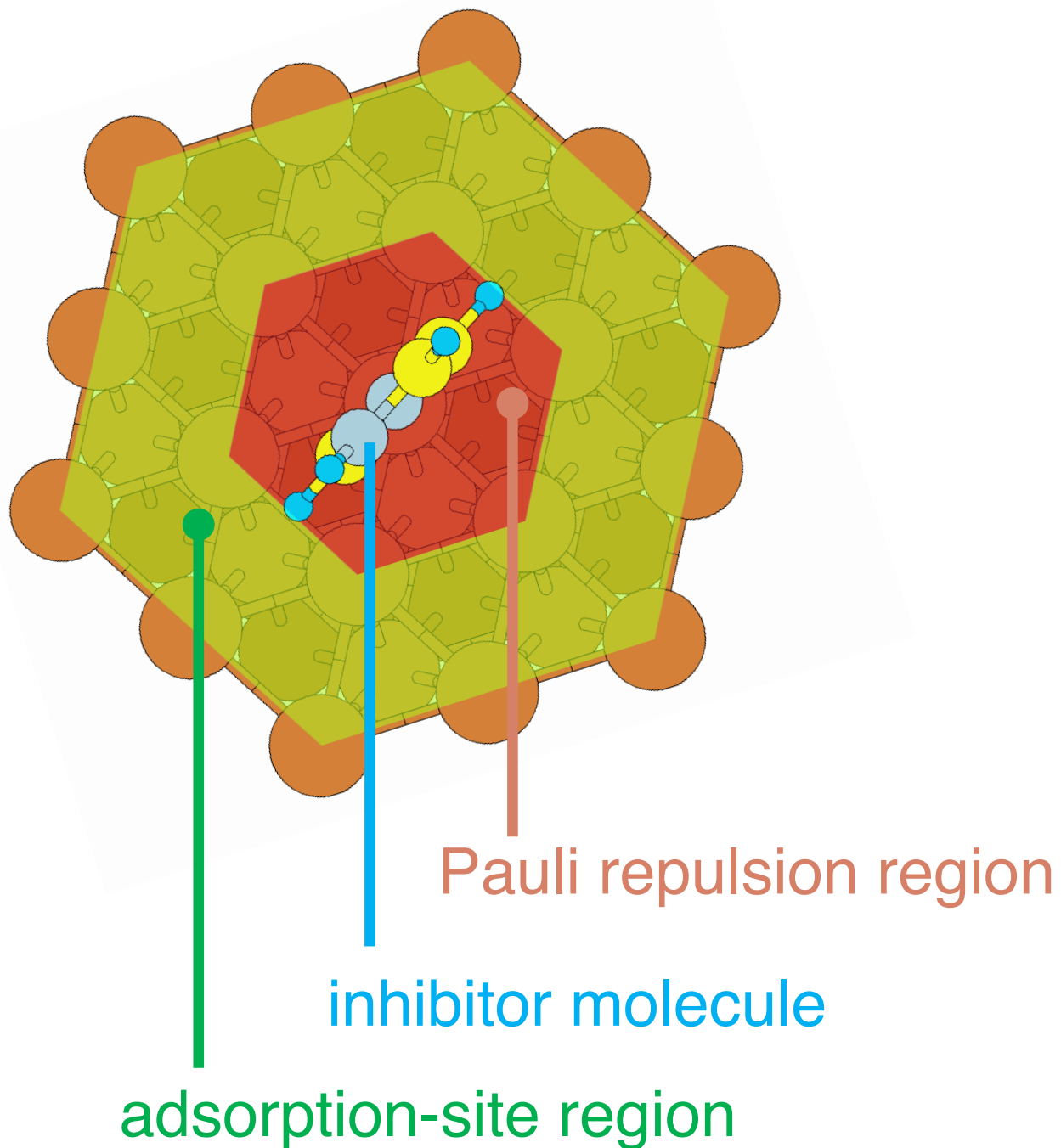
Cl

typically involved in
cathodic corrosion
reactions

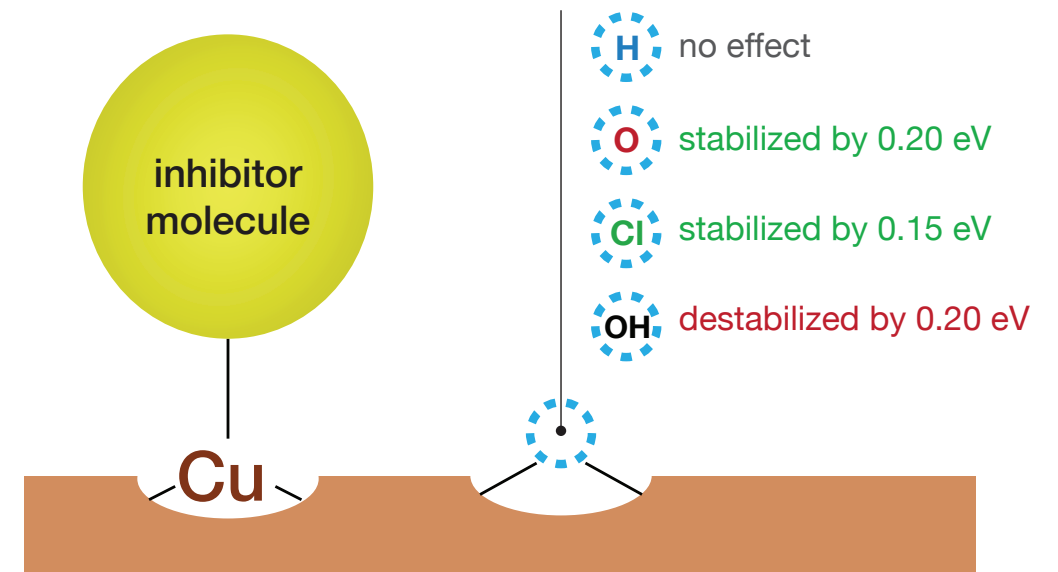
corrosion
activator

2.

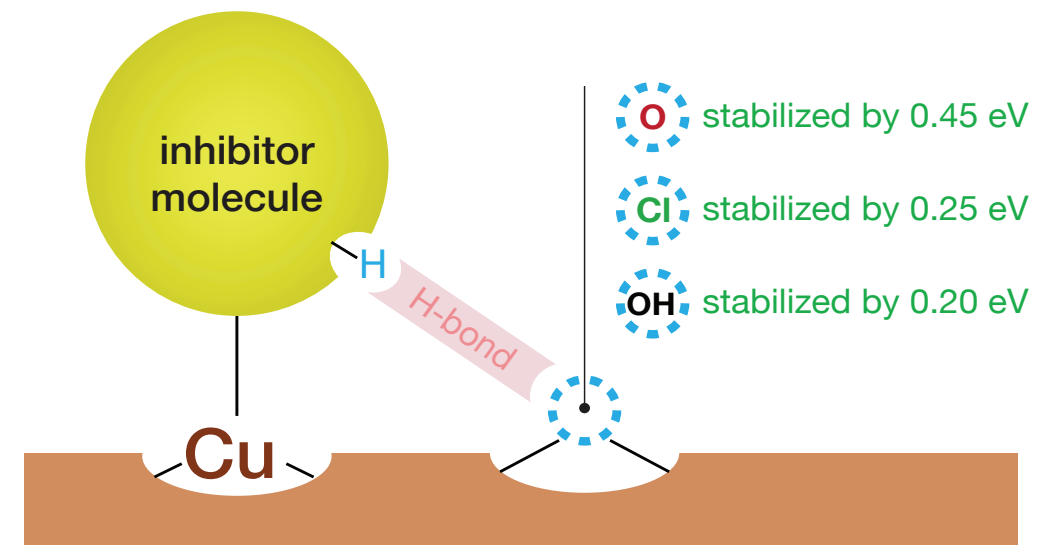
How are we doing it?



Effect of inhibitor on other species

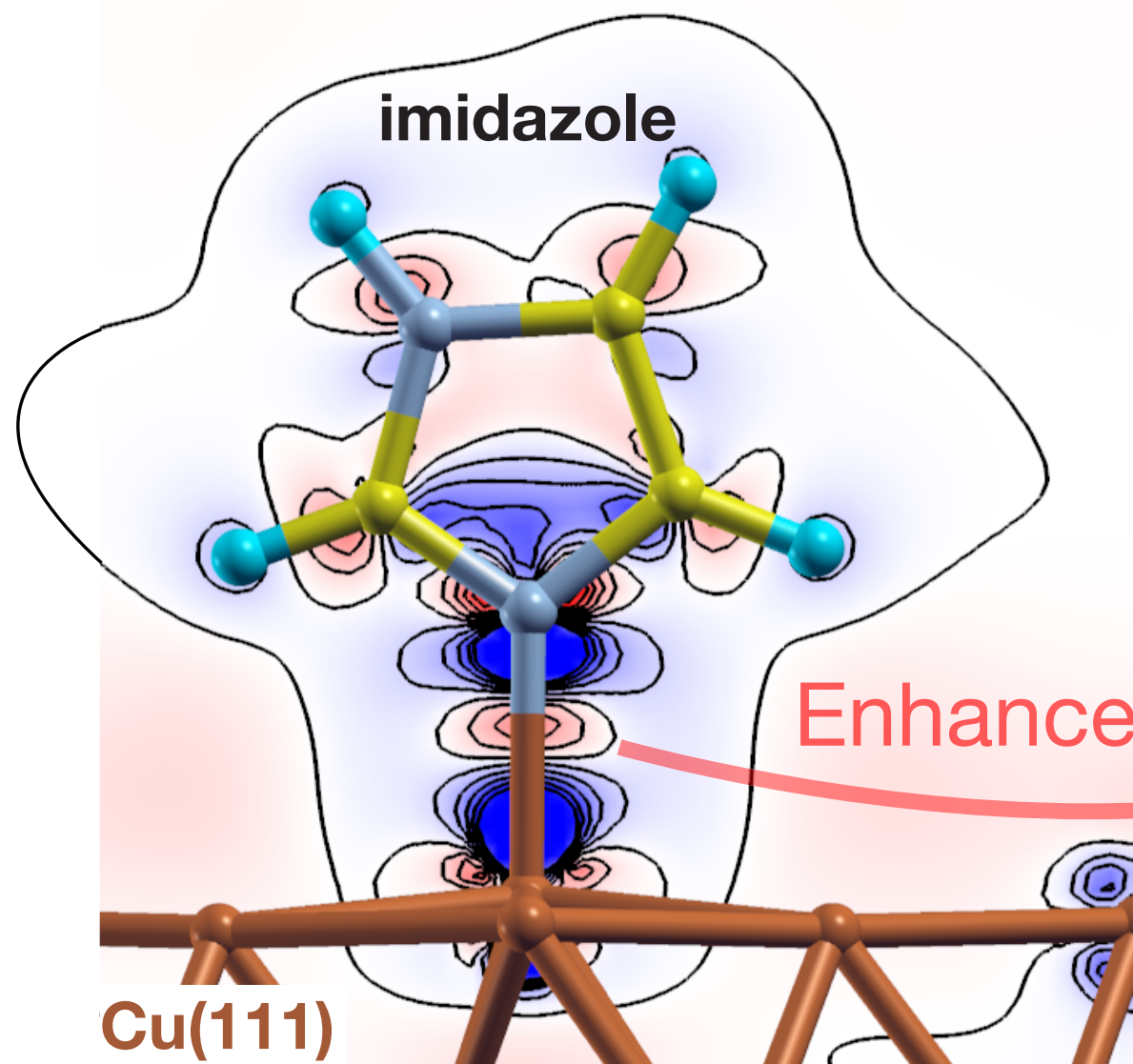


Effect ... when H-bond forms

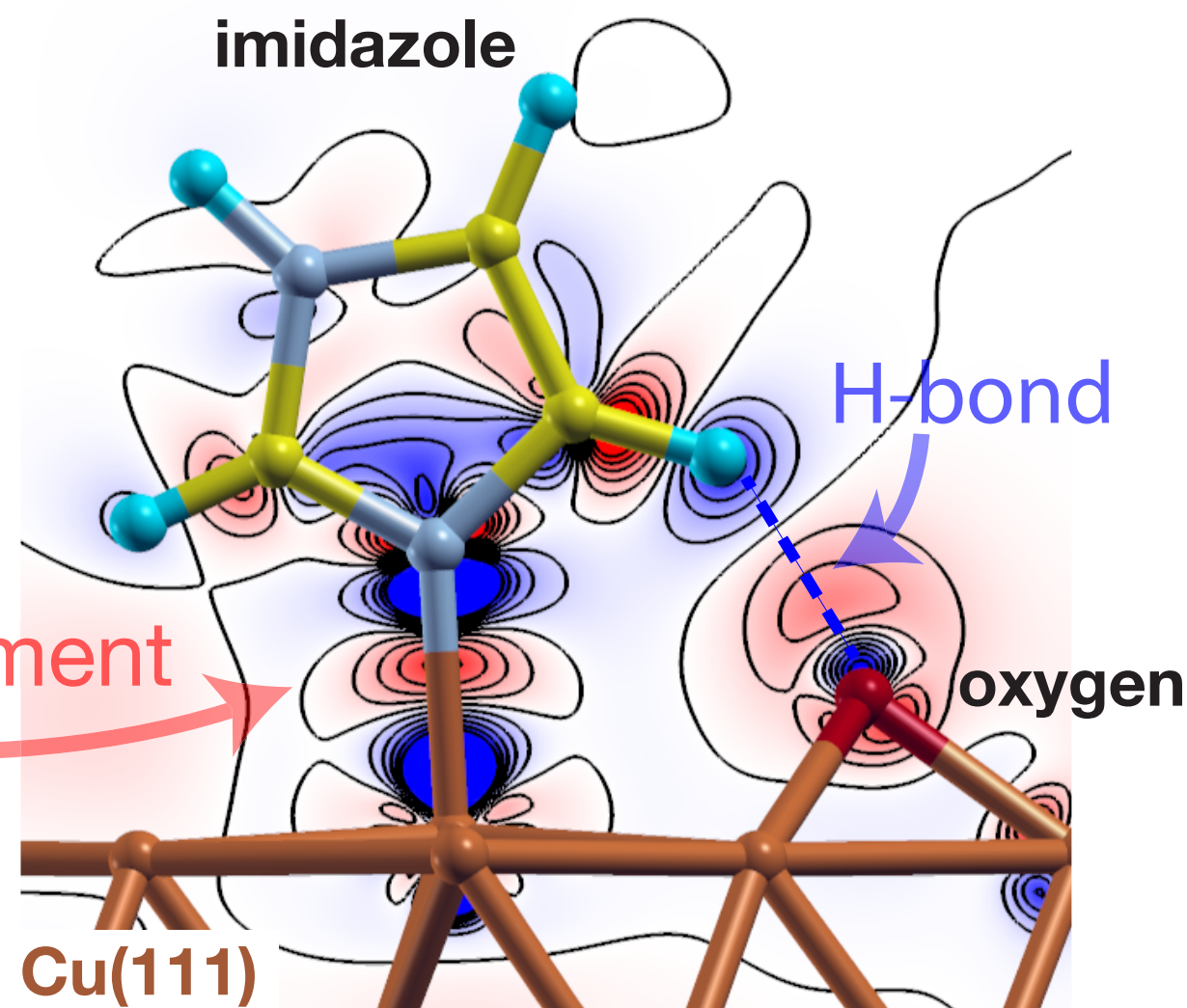


3.

What we discovered so far?



Charge density difference



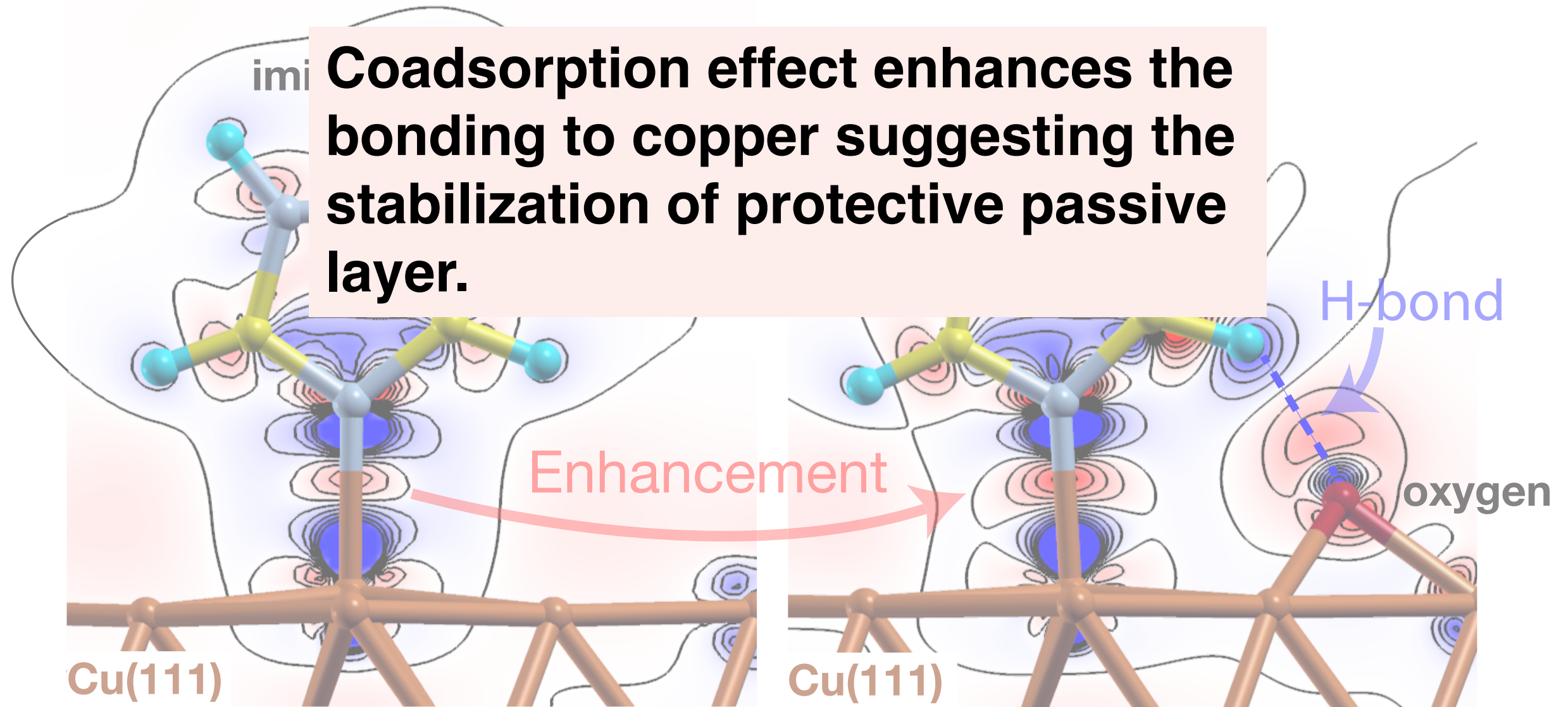
■ electron excess

■ electron deficit

3.

What we discovered so far?

Coadsorption effect enhances the bonding to copper suggesting the stabilization of protective passive layer.



Charge density difference

■ electron excess

■ electron deficit

THANK

YOU

Cordially invited
to poster number

27

The role of small coadsorbates on adsorption of azole molecules on copper surfaces



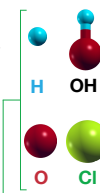
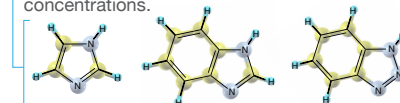
Matjaž Dlouhy^{1,2}, Anton Kokalj^{1,2}

¹ Department of Physical and Organic Chemistry, Jožef Stefan Institute, Jamova c. 39, 1000 Ljubljana, Slovenia

² Jožef Stefan International Postgraduate School, Jamova c. 39, 1000 Ljubljana, Slovenia

1. Introduction

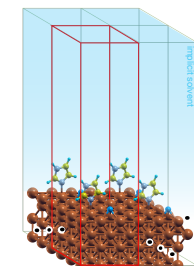
Corrosion inhibitors are substances with the ability to reduce corrosion rate already at very low concentrations.



Aim: Evaluate how some coadsorbed corrosion relevant species affect intermolecular interactions of adsorbed azole molecules.

2. Method

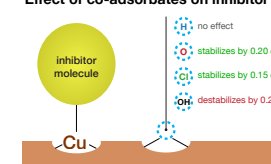
- computational method: DFT with GGA-PBE functional
- basis set: plane-waves with ultra-soft pseudopotentials
- program package: Quantum ESPRESSO, XCrySDen
- surface model: periodic multi-slab model of Cu(111)



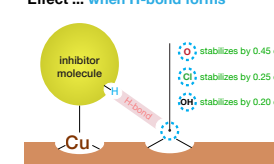
3. Results



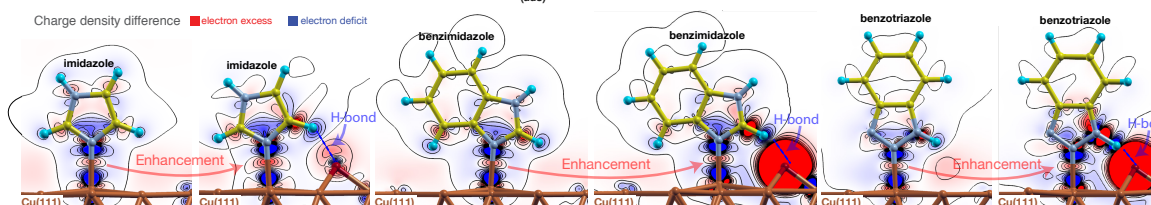
Effect of co-adsorbates on inhibitor



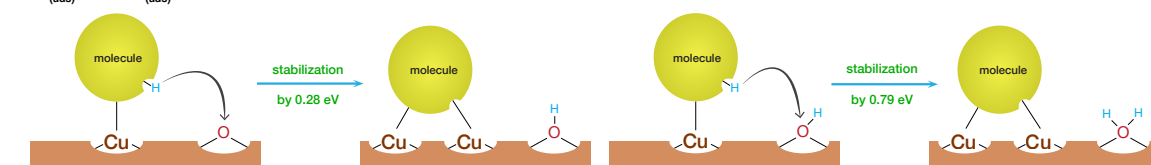
Effect ... when H-bond forms



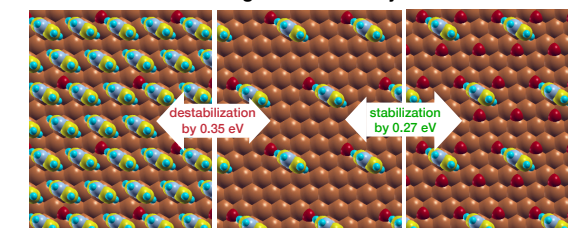
Enhancement of inhibitor-surface bonding by nearby $O_{(ads)}$



$O_{(ads)}$ and $OH_{(ads)}$ promote deprotonation of inhibitors resulting in a more stable state.



Effect of surface coverage on the stability of inhibitor molecule



4. Conclusion

Azole corrosion inhibitors affect the adsorption of corrosion relevant species on the surface

- $O_{(ads)}$ stabilizes the inhibitor molecule the most
- $Cl_{(ads)}$ stabilizes to lesser extent compared to $O_{(ads)}$
- $OH_{(ads)}$ destabilizes unless H-bond forms
- $H_{(ads)}$ does not affect the coadsorbed inhibitor

About the first author

Matjaž Dlouhy is a PhD student at Jožef Stefan Institute. He currently studies by DFT modelling the interaction of corrosion inhibitors and other species with surfaces under supervision of dr. Anton Kokalj.



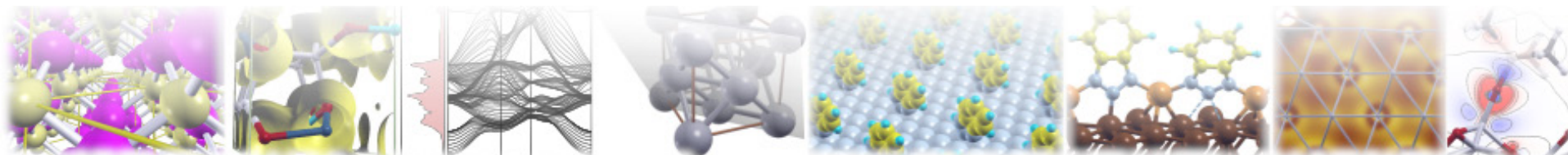


QUANTUMESPRESSO

September 15–20, 2019

Ljubljana, Slovenia

Summer School on Advanced Materials and Molecular Modelling



LET'S CONTINUE IN THE LOBBY DOWNSTAIRS.



QUANTUM ESPRESSO
FOUNDATION



DRIVING
THE EXASCALE
TRANSITION



Jožef Stefan
Institute
Ljubljana, Slovenija



Centre Européen de Calcul Atomique et Moléculaire



Imagine. Build. Succeed.